J. Opt. B: Quantum Semiclass. Opt. **1** (1999) R23–R45. Printed in the UK PII: S1464-4266(99)04404-3

PhD TUTORIAL

Optical lattices: cold atoms ordered by light

L Guidoni† and P Verkerk‡

Laboratoire Kastler Brossel, Département de Physique de l'Ecole Normale Supérieure, 24, rue Lhomond, F-75231 Paris Cedex 05, France
and
Laboratoire de Physique des Lasers, Atomes et Molécules, Centre d'Etudes et de Recherche Lasers et Applications, Université des Sciences et Technologies de Lille, UFR de Physique, Bâtiment P5, F-59655 Villeneuve d'Ascq Cedex, France

E-mail: `Philippe.Verkerk@univ-lille1.fr`

Received 19 May 1999, in final form 27 July 1999

Abstract. We present here an introduction to optical lattices starting from the basic concepts of laser cooling of neutral atoms. Ordered structures, composed of cold atoms in an interference pattern, are then described, with a particular emphasis on the basic mechanism called Sisyphus cooling. Afterwards, we introduce the basic elements of the main physical problem (an atom moving in a spatially modulated electromagnetic field) and we make a concise description of the various theoretical approaches that have been introduced in the literature in order to solve that problem. Finally, we report a detailed list of the multiple diagnostic tools that have been developed by physicists in order to investigate the static and dynamical properties of these systems. The new developments and the perspectives of the research field on optical lattices are then quickly discussed and conclude this introductory review.

Keywords: Laser cooling, Sisyphus cooling, optical lattice, pump-probe spectroscopy, Bragg diffraction

1. Introduction

Atomic physics traditionally deals with the electronic states of atoms. In particular, spectroscopic studies of atomic gases allow the precise determination of the energy separation between internal states and, therefore, the definition of time and frequency standards and the determination of the values of fundamental constants [1]. From this point of view, the presence of the atomic translational degrees of freedom can be viewed as a limiting factor because it introduces inhomogeneous and homogeneous line-widths for gaseous atomic samples. In the last two decades, the availability of tunable laser sources has allowed a very fine control of the light–atom interaction, introducing the new concepts of laser manipulation and laser cooling of neutral atoms [2–4]. The translational (or 'external') degrees of freedom have become more and more well controlled, control that culminated with the observation of Bose–Einstein condensation in dilute gas systems [5]. In that case a macroscopic atomic sample is described by a single wavefunction (including internal and external degrees of freedom).

† Present address: IPCMS, Unité mixte 7504 CNRS-ULP-ECPM; 23, rue du Loess, 67037 Strasbourg Cedex, France.
‡ Author for correspondence. Permanent address: Laboratoire PhLAM, UFR de Physique, Bat. P5, USTL, F-59655 Villeneuve d'Ascq Cedex.

This manipulation of the external state includes the creation of 'optical potentials'. In fact, when an atom interacts with a laser beam, the energy of its internal states depends on the light intensity; therefore a spatially dependent intensity induces a spatially dependent potential energy. If such a modulation is obtained with the interference of several laser beams, the resultant optical potential 'seen' by the atoms will display several 'optical potential wells' separated by a distance of the order of the laser wavelength. The depths of the optical potential wells that can be obtained in an experiment are in the mK range. Nevertheless, these relatively shallow potentials are compatible with the extremely low temperatures attainable with laser-cooling techniques. A new class of physical system has been therefore developed: the 'optical lattices' or 'light-bound atomic lattices' [6–8]. In these systems a cloud of laser-cooled atoms, interacting with several laser beams, becomes ordered while still preserving the character of a gas.

The atomic gas interacting with a spatially modulated optical potential displays a striking similarity to the electron gas affected by the ion-lattice potential in a solid crystal. This similarity, associated with the tunability of an optical potential, allowed the observation of several phenomena due to the band structure, shared between optical lattices and solid crystals: Bloch oscillations [9], Wannier–Stark ladders [10],

Zener tunnelling [11], dynamic band suppression [12]. These results show clearly that the optical lattices can play a prominent role in the comprehension of quantum transport phenomena [13].

Another very important aspect of optical lattices is represented by atomic lithography [14, 15]. In this case the control of atomic motion is applied to the deposition of ordered patterns on a substrate of technological interest. The spatial resolutions that can be attained are comparable to those obtained by electron-beam lithography with all the advantages of a parallel process. Moreover, the possibility of multi-atomic deposition opens the way to very interesting future applications.

This PhD tutorial is intended to be an introduction to this fast-developing field of optical lattices. A short review of laser-cooling techniques will precede the detailed description of bright optical lattices together with the main theoretical approaches that have been used to describe these systems. Finally, a quick description of several experimental diagnostics (with their theoretical explanation) will conclude the manuscript. Even if this tutorial is necessarily not complete, all the new trends that are now developing in this field are cited, allowing the reader to address the more specialized bibliography when a thorough search will be needed.

2. Laser cooling and the Sisyphus effect

2.1. Cooling atoms with light

Cooling atoms by using their interaction with an electromagnetic field flows directly out of fundamental conservation principles. Momentum conservation during the emission or the absorption of a photon plays an essential role in every laser-cooling scheme. The quantum mechanical picture of an atom usually separates the internal electronic states from the external degrees of freedom. Laser cooling is obtained when an atom, in a gas, loses its translational energy (associated with the motion of the centre of mass) because of repeated transitions between two internal states. Such cycles are obtained by irradiating the atom with a laser beam (a monochromatic, intense and coherent electromagnetic field). The frequency $\omega_L = 2\pi c/\lambda_L = k_L c$ of this laser beam must satisfy the relation

$$\hbar\omega_L \simeq \Delta E = \hbar\omega_0,$$

where ΔE is the energy separation between two internal states of the atom†.

Internal states: the two-level atom. The simplest atom we can imagine has just two levels (the ground state $|g\rangle$ and the excited state $|e\rangle$) and we consider these two levels interacting with a quasi-resonant beam. This physical system (two-level atom interacting with a light field) is completely described by the following parameters:

† In some laser-cooling configurations multiple laser beams at different frequencies can excite several atomic transitions. Even these more complicated situations are still well described by this basic idea of repeated internal cycles that induce a net decrease of external energy.

ω_0: angular frequency of the atomic transition,
Γ: natural width of the excited state,
$\Delta = \omega_L - \omega_0$: detuning between laser beam and atomic transition,
Ω: the Rabi frequency, carrying information about the laser intensity (I) and about the atom–field coupling (in particular, $\Omega^2 \propto I$).

The saturation parameter is also very important:

$$s = \frac{\Omega^2/2}{\Delta^2 + \Gamma^2/4}.$$

We consider now a two-level atom at rest in a travelling plane wave: after a transient time of the order of Γ^{-1}, the excited-state population takes its stationary value $\Pi_e = \frac{1}{2}s/(1+s)$. In this situation the atom emits $\Pi_e\Gamma$ spontaneous photons per time unit, every spontaneous emission being preceded by the absorption of a laser photon. It is very useful to consider the low-saturation regime defined by the condition $s \ll 1$. In this case, $\Pi_e \simeq s/2 \ll 1$ and the atom spends most of its time in the ground state.

External states: the recoil and Doppler cooling. We can now introduce the external degrees of freedom in the description of the atom–field interaction. The momentum conservation principle states that, every time an atom of mass M absorbs a photon of wavevector $\boldsymbol{k}$, a recoil effect arises that pushes the atom along the $\boldsymbol{k}$ direction. When the photon is emitted along $\boldsymbol{k}$, the recoil is directed in the $-\boldsymbol{k}$ direction. The velocity acquired by the atom, as a consequence of the absorption of a resonant photon, is called the 'recoil velocity' v_{rec} and $v_{rec} = \hbar|\boldsymbol{k}|/M = \hbar k_0/M$. The corresponding kinetic energy is called the 'recoil energy' $E_{rec} = \hbar^2 k_0^2/2M$; such kinetic energy can be also associated with a 'recoil temperature' $T_{rec} = M v_{rec}^2/k_B$. The atom placed in a travelling wave always absorbs photons with a well determined direction but emits photons in a random direction. The net average result is a force directed along the laser beam that is called the radiation pressure force (or dissipative force). This force can be calculated just by taking the rate of spontaneous photon emission times the momentum carried by a single photon:

$$\boldsymbol{\mathcal{F}}_{dissip} = \Gamma\Pi_e\hbar\boldsymbol{k}_L = \frac{\Gamma}{2}\hbar\boldsymbol{k}_L\frac{s}{1+s}.$$

In the low-saturation regime this expression becomes:

$$\boldsymbol{\mathcal{F}}_{dissip} \simeq \frac{\Gamma}{2}\hbar\boldsymbol{k}_L s = \frac{\Gamma}{4}\hbar\boldsymbol{k}_L\frac{\Omega^2/\Gamma^2}{\Delta^2/\Gamma^2 + \frac{1}{4}}. \qquad (2.1)$$

Even if the momentum carried by a single photon is usually very small (with respect to the thermal atomic momentum) the excited state is so short-lived that many photons can be exchanged during the time unit. The resulting force is therefore not negligible at all and, for example, in the case of a caesium atom with $\Delta = -\Gamma/2$ and $\Omega = \Gamma$ ($s = 1$) its value is 3000 times the force of gravity. The first experimental evidence of radiation pressure was the bending of an atomic beam trajectory obtained with resonant light in 1933 [16]. It is interesting to note that the experiment was

realized before the development of laser sources. The ability of changing the atomic momentum allows the acceleration (and the slowing down!) of atomic beams. However it does not allow, by itself, the cooling of an atomic gas. In order to cool down, in fact, we have to be capable of narrowing the velocity distribution instead of just changing its mean value. Every laser-cooling scheme has to slow down the rapid atoms without affecting the slow ones. The first scheme proposed to obtain this effect is called 'Doppler cooling', and was proposed in 1975 both for neutral atoms [17] and for trapped ions [18]. The Doppler-cooling mechanism is based on the Doppler effect: a moving atom with its velocity v aligned on a beam direction 'sees' an effective laser frequency scaled by the factor $1 \mp v/c$ (the sign $\mp$ corresponding to parallel/anti-parallel motion, respectively). In order to narrow, for instance, the z velocity distribution, the atoms are placed in a pair of counter-propagating beams aligned along the z axis, both red-detuned with respect to the atomic transition ($\Delta < 0$). In this situation, a moving atom experiences a net radiation pressure force against its motion. The radiation pressures associated with the two beams are in fact unbalanced because of the frequency dependence of the force (2.1):

$$\mathcal{F}_z = \frac{\Gamma}{2}(s_+\hbar k_{L^+} - s_-\hbar k_{L-}) \simeq -v_z\hbar k_L^2 \frac{\Omega^2}{\Gamma^2}\frac{\Delta/\Gamma}{(\Delta^2/\Gamma^2 + \frac{1}{4})^2}$$

(this expression is valid in the low-saturation regime and for $|k_L v_z| \ll \Gamma$). The atoms with a zero velocity along the z direction are submitted to a force that averages to zero because the radiation pressures of the two beams exactly compensate. If three such pairs of beams are oriented along the Cartesian axes, the three-dimensional (3D) cooling of an atomic gas cloud becomes possible. In this situation the kinetic energy of the atoms is dissipated during the absorption and spontaneous emission cycles. During these cycles an atom always absorbs red-detuned photons, but it emits, on average, photons that are not detuned with respect to the atomic transition (and are therefore more energetic). It is very important to note that this kind of cooling process produces an atomic sample that is cold but not necessarily dense. Such a system is usually called an 'optical molasses' due to the presence of a viscous force that slows down the atoms without the presence of a restoring force eventually able to gather them.

Doppler cooling has been studied in detail from the theoretical point of view [19] and we will cite here some fundamental results.

- The equilibrium velocity distribution of the atomic cloud is a Maxwell–Boltzmann distribution (it is therefore possible to define a temperature of the sample). The distribution width is essentially determined by the random recoil momentum received by the atom during the spontaneous emission processes.
- The minimum achievable temperature $k_B T_{Dopp} = \hbar\Gamma/2$ is obtained in the low-intensity limit and with $\Delta = -\Gamma/2$.
- Only the atoms with a velocity v that fulfils the relation $|k_L v| \simeq \Gamma$ (Doppler shift of the order of the natural width) can interact with the beams and are then cooled down. It is therefore possible to define a 'velocity capture range' associated with Doppler cooling: $v_{capt} \simeq \Gamma/k_L$.

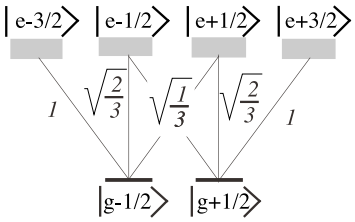

Figure 1. Energy-level diagram and Clebsch–Gordan coefficients for a $J_g = \frac{1}{2} \rightarrow J_e = \frac{3}{2}$ transition.

The first optical molasses was realized experimentally in 1985 with sodium atoms cooled with a dye laser [20]; other analogous experiments were soon performed. All the experiments seemed to confirm the theoretical results obtained within the two-level-atom approximation.

The absence of a restoring force imposes strong limitations on the density and on the lifetime of the optical molasses. A great effort was therefore devoted to find a beam configuration that could eventually associate cooling and trapping, both obtained by radiation pressure forces. Unfortunately, after some proposals [21], the 'optical Earnshaw theorem' [22] demonstrated that it is impossible to trap a two-level atom in a stable configuration just by using the radiation pressure force induced by several time-independent laser beams.

Angular momentum conservation: Zeeman sub-levels and optical pumping. The two-level-atom approximation correctly describes the Doppler-cooling mechanism. Nevertheless, experiments necessarily deal with more complicated atoms and these systems may exhibit some new interesting features. The next step is therefore to analyse the atom–field interaction in the case of atoms (for example, the alkali atoms) which have multiple Zeeman sub-levels in their ground state. Two new phenomena have now to be taken into account, both flowing out of angular-momentum conservation principle: selection rules concerning the polarization of the photons and Clebsch–Gordan coefficients. First, the absorption of a circularly polarized photon σ^+ (σ^-) can only increase (decrease) the internal quantum number m by one unit†; the absorption of a π polarized photon leaves m unchanged. Second, the coupling between the ground state sub-levels $|g, m\rangle$ and the excited state sub-levels $|e, m'\rangle$ depends on the polarization state of the exchanged photon. As a useful example we consider in detail the case of a $J = \frac{1}{2} \rightarrow J' = \frac{3}{2}$ transition (figure 1). An atom initially in the $|g, +\frac{1}{2}\rangle$ state can absorb a σ^+ photon ending up in the $|e, +\frac{3}{2}\rangle$ state, or absorb a σ^- photon ending up in the $|e, -\frac{1}{2}\rangle$ state or absorb a π photon ending up in the $|e, +\frac{1}{2}\rangle$ state. For the same intensity of the three polarization components, the first case is three times

† We use here the standard notation denoting with m the eigenvalues of the operator J_z, projection of the total angular momentum J along the z axis. The quantization axis z has to be imposed on the atom, for example by the presence of a homogeneous magnetic field.

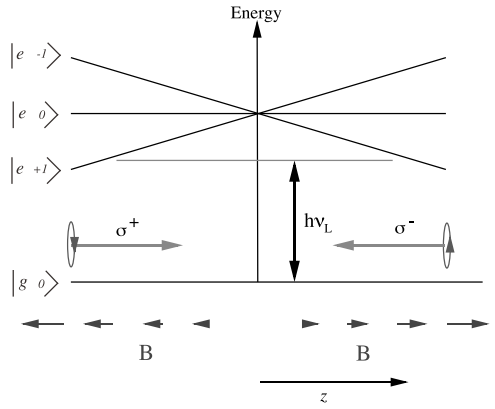

Figure 2. Working scheme of a magneto-optical trap (MOT). A hypothetical atom on a $J_g = 0 \rightarrow J_e = 1$ transition placed in an inhomogeneous magnetic field $\boldsymbol{B} = b\boldsymbol{z}$ under the action of two counter-propagating, red-detuned laser beams. The two beams have opposite circular polarizations that are chosen in order to bring closer to resonance (by the Zeeman effect) the beam that propagates toward the origin ($z = 0$).

more probable than the second one and one-and-a-half times more probable than the third one. Once in the excited state, the atom decays to the ground state through the emission of a spontaneous photon. The decay probabilities also depend, *via* the Clebsch–Gordan coefficients, on the emitted photon polarization. These two features are the foundations for the phenomenon of 'optical pumping' [23]: the atom–field interaction can impose a stationary population of the Zeeman sub-levels†. Let us take again the preceding example of a $J = \frac{1}{2} \rightarrow J' = \frac{3}{2}$ transition. Our atom interacting with a purely σ^+-polarized beam will eventually cycle between the outermost Zeeman sub-levels $|g, +\frac{1}{2}\rangle$ and $|e, +\frac{3}{2}\rangle$. The characteristic time τ_p required to reach this situation is called the optical pumping time.

Magneto-optical trap. In the case of multi-level atoms, the optical Earnshaw theorem, forbidding a radiation-pressure-based stable trap, does not apply. Starting from this statement [24], it is possible to search for a mechanism analogous to Doppler cooling but affecting the position space instead of the momentum space. In fact, the following idea is the basis of a trap: we have to push towards a 'centre' only those atoms that moved away. This means that only the radiation pressure due to the beam propagating towards the escaping atom has to be selectively increased. This position selectivity can be obtained either by changing the stationary populations of the Zeeman sub-levels with optical pumping [24] or by inducing a shift of the energy levels with an inhomogeneous magnetic field. The last option is the basis of the magneto-optical trap (MOT), the most widely used laboratory tool for the production of cold atom samples.

For the sake of simplicity, we consider a fictitious atom of zero spin on a $J = 0 \rightarrow J' = 1$ transition placed in a region where a static magnetic field $\boldsymbol{B} = b\boldsymbol{z}$ is present. Two beams counter-propagate along the z axis with a σ^+ and σ^- polarization (figure 2). As in the case of Doppler cooling, the laser frequency is red detuned; a friction force is therefore applied to the atoms. For an atom at rest in $z = 0$, the radiation pressure forces due to the two beams exactly compensate. In contrast, because of a Zeeman shift of the excited states, an atom at rest but displaced towards the $+z$ direction becomes more sensitive to the σ^- polarized beam and less sensitive to the σ^+ beam (figure 2). The Zeeman shift decreases the detuning of the beam that pushes towards the origin, and increases the detuning of the beam that pushes away: thus we have a restoring force. If the atom is located in the $-z$ half-space, the Zeeman shift is reversed, and the σ^+ beam radiation pressure (instead of the σ^- one) becomes predominant. Such a system can be generalized to 3D, just by using a quadrupolar magnetic field and three pairs of counter-propagating beams.

The first MOT was realized with sodium atoms on a $2 \rightarrow 3$ transition [25]. This trap was filled by an atomic beam slowed down by a laser. The features of this system were exceptional: 10^6 atoms were confined in a 0.32 mm diameter region with a life-time of 120 s and a temperature of the order of 500 μK. The magnetic field gradient was of the order of 10 G cm^{-1} and the detuning $-2\Gamma \leqslant \Delta \leqslant -1\Gamma$. Some years later [26], the possibility was demonstrated of trapping and cooling in a MOT starting directly from a low-pressure vapour at room temperature. The experimental technique becomes in this case quite simple, allowing the multiplication of cold atom sources worldwide.

2.2. Sub-Doppler cooling and 1D Sisyphus effect

In 1988 a key experiment [27] demonstrated that the temperature obtained in optical molasses could become lower than the theoretical limit imposed by the Doppler model. This experiment was performed with sodium atoms on the $2 \rightarrow 3$ transition of the D_2 line, with mutually orthogonal polarizations for the three standing waves inducing the 3D cooling. Moreover, the temperature dependence versus the detuning Δ exhibited an opposite behaviour with respect to the behaviour predicted by Doppler-cooling theory: i.e., a monotonic temperature decrease with increase of the detuning from resonance.

Sub-Doppler cooling mechanisms. The explanation of such surprising results can only be obtained by considering the presence of multiple Zeeman sub-levels in the atomic transitions involved in the experiment. This theoretical description of these 'new mechanisms' was published independently by two research groups [28, 29] in 1989. The basic idea follows: when the electromagnetic field displays a position-dependent polarization, the optical pumping phenomena try to adapt the ground state of the atom to the local polarization of the field. If the atom moves and the spatial variations of the polarization are rapid (as in the case of stationary waves‡, where the spatial periodicity is imposed by the wavelength λ_L), this adaptation does not follow adiabatically the polarization. The non-adiabatic

† This situation is often described in terms of 'alignment' of the atomic state to an orienting field.

‡ In the following we will use the term 'stationary wave' (and sometimes the term 'interference pattern') in a more comprehensive way than usual. For instance, the polarization of the back-reflected beam could be changed.

transitions that arise are responsible for a new friction force and, therefore, a new cooling process.

The phenomenon of 'light shift' is the other fundamental element of the polarization gradient cooling mechanism. This energy shift of the atomic levels (a.c. Stark shift) has its origin in the interaction of the laser-induced dipole with the light field itself; the presence of this interaction induces an extra spacing between the energy levels. In the case of a two-level atom placed in a travelling wave, the light shift that affects the $|g\rangle$ state and the $|e\rangle$ state is:

$$\delta E_g = -\delta E_e = \hbar\Delta' = \hbar\Delta s/2. \tag{2.2}$$

It is interesting to stress that this energy shift is a coherent phenomenon completely independent of the excited-state population. In particular, it is possible to have strong light shifts with a negligible photon scattering rate (far-detuned regime). If multiple Zeeman sub-levels are present, the light shift of a ground state sub-level depends on its coupling with the excited state. In this case the local polarization of the light field can affect (through the Clebsch–Gordan coefficients) the light shift. When the light field intensity and/or polarization display spatial variations, the energy levels of the ground state are differently shifted depending on the spatial position of the atom. These energy shifts can be viewed as an effective potential energy that affects the external degrees of freedom of the atom (optical potential). It is important to note that in the very simple case of a stationary wave, the spatial variations of the optical potential are in the range of the wavelength λ_L. Moreover, in the case of a multi-level atom the light shift and the optical pumping act at the same time.

We will introduce the cooling mechanisms in a semi-classical frame: the external degrees of freedom are not quantized, although the full quantum treatment is sometimes possible [30]. We will also restrict ourselves to the low-saturation regime ($s \ll 1$), neglecting the light shift associated with the excited state. We will describe two 1D light-field configurations that have been studied in detail: the $\sigma^+ - \sigma^-$ configuration (used in the MOT) and the lin⊥lin configuration (the archetype of the optical lattice).

$\sigma^+ - \sigma^-$ molasses. In the $\sigma^+ - \sigma^-$ configuration we consider an atom on a $J = 1 \rightarrow J' = 2$ transition† interacting with a stationary wave obtained from two planes waves counter-propagating along the z axis. These waves have the same frequency ω_L, the same intensity I_0 and opposite circular polarizations. The two orthogonally polarized waves cannot interfere (in the usual meaning), so the intensity does not depend on the position. In fact, this stationary wave displays, for each z, a linear polarization and the polarization vector rotates around Oz following a linear helix with a pitch λ_L (corkscrew molasses). We have in this situation a polarization gradient of the light field without changes in ellipticity. In this particular situation, the light shifts of the Zeeman sub-levels do not vary with z and only the orientation phenomena are important. If we consider an atom at rest, and a red-detuned laser ($\Delta < 0$), the three ground state Zeeman sub-levels‡ have different populations and are differently light shifted: $|g, +1\rangle$ and $|g, -1\rangle$ have each a steady-state population of $\frac{4}{17}$ and a light shift $\Delta'_{\pm 1}$ while $|g, 0\rangle$ has a population of $\frac{9}{17}$ and a light shift of $\Delta'_0 = \frac{4}{3}\Delta'_{\pm 1}$).

The problem of a moving atom can be solved in a moving and rotating frame that leaves the atom at rest and the linear polarization direction fixed. This frame change introduces in the Hamiltonian an inertial term described by a fictitious homogeneous magnetic field in the z direction. If the atomic velocity is small, the effect of this magnetic field can be treated as a perturbation: the new eigenstates are linear superpositions of the three Zeeman sub-levels. It is now possible to calculate the stationary populations in this new basis and to write down the result in the laboratory frame. For a moving atom, a population difference between the $|g, -1\rangle$ and $|g, +1\rangle$ states arises:

$$\Pi_{+1} - \Pi_{-1} \propto k_L v/\Delta'_{\pm 1}.$$

This population difference is responsible for the friction force: for a red detuning ($\Delta < 0 \Rightarrow \Delta'_{\pm 1} < 0$), the moving atoms preferentially absorb photons in the wave that propagates against their motion. Because the friction force is strong even for low velocities, this mechanism produces samples colder than the Doppler-cooled samples. On the other hand, the velocity capture range is determined by the optical pumping time: several optical pumping cycles have to occur while the atom moves along a distance of the order of λ_L. A rough estimation of the velocity capture range is then $k_L v_{capt} \simeq \Gamma'$. The slowness of the optical pumping processes allows a strong friction but imposes a poor velocity capture range. The energy balance of the cooling mechanism is quite similar to the Doppler-cooling case: the spontaneously emitted photons are, on the average, blue detuned with respect to the absorbed photons and take away the thermal energy. It is interesting to note that the absence of an optical potential (reactive restoring force) is reflected by the absence of atomic density modulation at the wavelength scale. The description in terms of 'optical molasses' still works in this sub-Doppler-cooling configuration.

lin⊥lin configuration: Sisyphus cooling. In the lin⊥lin configuration, we consider an atom on a $J = \frac{1}{2} \rightarrow J' = \frac{3}{2}$ transition interacting with a stationary wave obtained with two plane waves that counter-propagate along the z axis having linear orthogonal polarizations. As in the preceding field configuration, the orthogonally polarized beams do not produce a spatial intensity modulation; in contrast however, the ellipticity of the light field is no longer constant. If we fix the z origin at a site where the two waves are in quadrature, the field polarization is circular, for instance σ^-. If we move by $\lambda_L/8$ in the positive direction, the two waves become π dephased (linear polarization). At $z = \lambda_L/4$ the waves are again in quadrature, but opposite to that of the origin (σ^+ polarization); at $z = 3\lambda_L/8$ the two waves are in phase (linear polarization orthogonal to the preceding one); finally, at $z = \lambda_L/2$ the polarization again becomes σ^-, as at $z = 0$ (figure 3(a)). This ellipticity gradient induces position-dependent light shifts for the two ground state Zeeman sub-levels $|g, +\frac{1}{2}\rangle$ and $|g, -\frac{1}{2}\rangle$; the spatial periodicity of this optical potential is therefore $\lambda_L/2$

† This mechanism works on every $J \rightarrow J+1$ atomic transition with $J \geqslant 1$.
‡ We choose the direction of the local field as the quantization axis.

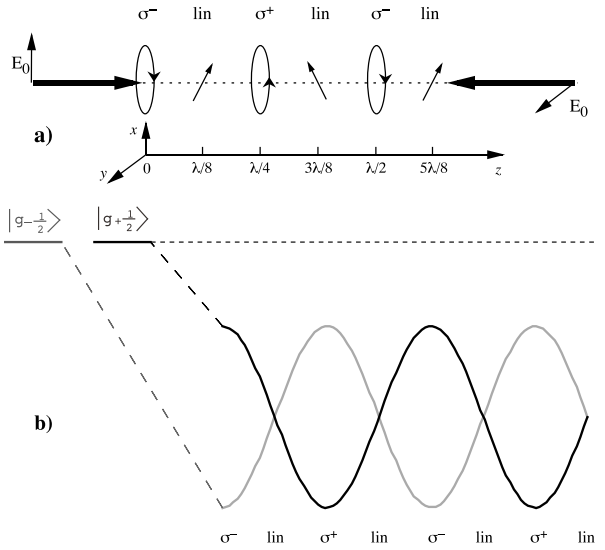

Figure 3. (*a*) lin⊥lin light-field configuration: the interference between two orthogonally polarized plane waves produces two classes of sites having opposite circular polarization with a spacing of $\lambda_L/4$. (*b*) The light shifts of the Zeeman sub-levels (here in the case of a $\frac{1}{2} \rightarrow \frac{3}{2}$ atomic transition) are position dependent due to the fact that the couplings vary with polarization (Clebsch–Gordan coefficients).

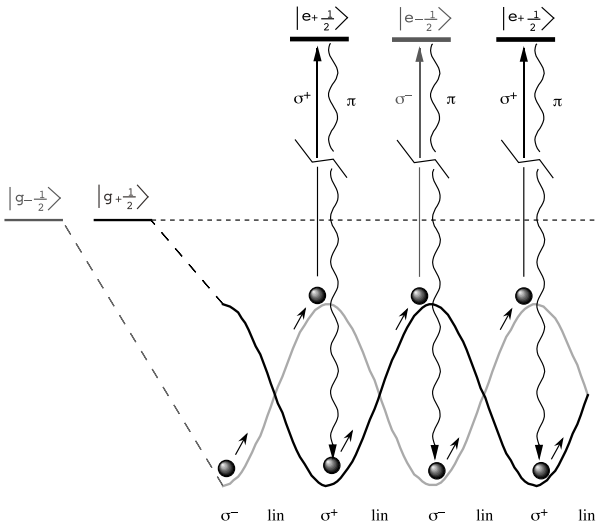

Figure 4. Perfect spatial correlation between optical pumping and light shift induces a loss of kinetic energy for an atom moving in a lin⊥lin light-field configuration: the atom always climbs the hills but never goes down freely (Sisyphus effect).

(figure 3(*b*)). We start by considering an atom at rest and a red detuning ($\Delta < 0$): the optical pumping process populates the two Zeeman sub-levels differently depending on the z position. In particular, the most light-shifted sub-level is always the most populated one. For instance, if we consider a σ^+ polarized site, the negative light shift is maximum for $|g, +\frac{1}{2}\rangle$ and the atom is optically pumped in this state. For an atom with non-zero velocity this situation is slightly modified: at a given time the atom can be in a sub-level that does not correspond to the most probable sub-level in the stationary case. This is because the optical pumping time is finite and the orientation can be a relatively slow process. In this situation, when an optical pumping cycle occurs, the potential energy of the atom will preferentially decrease. This is, once again, because the most populated state is also the most light shifted. If we consider, in particular, an atom with a velocity such that $v/\Gamma' \simeq \lambda_L/4$, we can easily see that the most probable trajectory consists of multiple climbing of the optical potential hills without any descent (figure 4). The dissipation mechanism is quite clear in this cooling mechanism: the kinetic energy first becomes potential energy during the climb-up; when the optical pumping cycle occurs, the potential energy decreases because the emitted photon is more energetic than the absorbed photon. The energy difference between the two photons is of the order of $\hbar\Delta'$. Based on this consideration, an estimate of the friction coefficient is straightforward: the power dissipated by a friction force is given by $P = -\alpha v^2$; an atom with a velocity $v \simeq \Gamma'/k_L$ loses the energy $\hbar\Delta'$ in a time of the order of $1/\Gamma'$. We can then write $\alpha \simeq -\hbar k_L^2 \Delta/\Gamma$. As in the case of the $\sigma^+ - \sigma^-$ molasses, the velocity capture range is imposed by the wavelength λ_L and the optical pumping time $1/\Gamma'$. If the atom is too rapid, the optical pumping cycles occur at sites that are not correlated with the optical potential and the cooling process loses its efficiency.

With respect to the preceding cooling mechanisms, the Sisyphus cooling displays a completely new feature. In the stationary state, the atomic sample becomes not only cold but also ordered. From a semi-classical point of view, when the kinetic energy of the atom becomes lower than the optical potential barrier, the atom oscillates around an equilibrium position (a σ^+ or a σ^- site). This system, an ordered sample of atoms cooled in a modulated optical potential induced by the interference pattern of several laser beams, is called an 'optical lattice'.

Sub-recoil cooling, Raman cooling. As we have seen, in the standard Sisyphus mechanism the atoms are cooled down and localized at sites where their interaction with the laser field is maximum. This situation affects the minimum steady-state temperature, because the momentum distribution width is determined by a dynamical equilibrium between the dissipation mechanism and the heating induced by photon scattering [28]. In order to overcome that limitation, some extensions of the Sisyphus mechanism have been proposed [31–33] that work on a $J \rightarrow J' = J$ or $J \rightarrow J' = J - 1$ transition with a blue detuning ($\Delta > 0$). In these situations the atoms are accumulated in states that have a minimum photon-scattering rate (Gray optical molasses). Anyway, the polarization-gradient cooling is based on spontaneous processes: a friction force is always associated with an inelastic photon scattering. Therefore, the steady-state momentum distribution cannot become narrower than the recoil momentum $\hbar k_L$. Two completely different laser-cooling mechanisms are able to break down this limitation: velocity-selective coherent population trapping (VSCPT) [34, 35] and Raman cooling [36, 37]. VSCPT is based on a quantum interference mechanism that creates an atomic state not coupled to the laser field. The atoms are trapped in this state which has a zero average momentum and can therefore be cooled down to very low temperatures ($T_{rec}/800$ for He atoms [38]). This mechanism cannot be

interpreted in terms of a friction force: the cooling is obtained through a diffusion process in momentum space that brings the atoms into a 'trap' where they cannot interact with the laser field.

Raman cooling is another sub-Doppler mechanism and, contrary to VSCPT, it is often associated with optical lattice experiments. The basic principles are the following: an atom with two stable states (e.g. two hyperfine sub-levels of the ground state) can flip between these states under the action of a 'Raman pulse'. Such a pulse consists of the superposition of two detuned coherent laser pulses with an adjustable temporal duration. The detuning is such that the frequency difference is nearly resonant with the energy separation between the stable states. The average frequency is chosen in order to minimize the spontaneous photons due to the presence of an excited state. If we consider atoms at rest, the width of a 'Raman transition' is virtually limited just by the pulse time duration through the Fourier transform (the two ground states are stable). For moving atoms, the Doppler effect introduces a velocity dependence on the resonance condition. It is therefore possible to selectively flip only the atoms belonging to a precise velocity class determined by the detuning and the pulse temporal profile. During this flip transition, there is a net momentum transfer to the atom due to the absorption-stimulated emission cycle. In the case of counter-propagating Raman beams this transfer is $2\hbar k_L$ and can be used to bring the rapid atoms towards a zero average momentum, without affecting the already cold atoms. This process can be iterated using multiple Raman-pulse sequences, obtaining 1D temperatures of 4 nK for free caesium atoms [37]. The main interest of the Raman cooling is its energy selectivity (that is, a velocity selectivity for free atoms). This feature allows the direct cooling of atoms in a non-dissipative trap.

3. Optical lattices

As mentioned earlier, the Sisyphus effect is a mechanism that can cool and trap the atoms in an interference pattern. Indeed, in this field configuration, the presence of a friction force spatially correlated with the optical potential naturally fills the potential wells and creates a stationary spatial density modulation. The description of this system naturally splits into a Hamiltonian part (conservative atom–field interaction) and a dissipative part that takes into account the cooling [39]. Even if the first examples of optical lattices have been obtained with this configuration [40, 41], it is also possible to separate the trapping and the cooling processes. In particular, once the cooling is obtained, the photon scattering rate can be strongly reduced in order to allow a free quantum evolution of the atomic wavefunction (which collapses every time a spontaneous emission process arises) [9]. It is therefore very useful to study the optical potential alone (and deduce, for instance, the symmetry properties of the system) and analyse the whole-system properties later. This approach ensures a high degree of generality: even the optical lattices operating in the 'far-detuned' regime can be described in this way. However, it is important to recall that the optical lattices have to be filled with atoms and that this filling is frequently obtained with dissipative processes. To predict most of the dynamical and static characteristic observables, it is necessary to take into account the details of the relaxation mechanisms eventually operating in the optical lattice.

3.1. 1D Sisyphus optical potentials.

The optical potential in the 1D lin⊥lin Sisyphus configuration is due to the interaction of the atom with the field of two plane waves, counter-propagating along the z axis, with the same intensity $I_0 = |E_0|^2$ and the same frequency ω_L. Taking the z axis as the quantization axis, we can write the total field as:

$$\boldsymbol{E}_L(z) = \tfrac{1}{2}E_0 \mathrm{e}^{-\mathrm{i}\omega_L t}\sqrt{2}[\boldsymbol{\varepsilon}_- \cos(k_L z + \phi) + \mathrm{i}\boldsymbol{\varepsilon}_+ \sin(k_L z + \phi)] + \mathrm{c.c.}, \tag{3.1}$$

where we have introduced the circular basis for the polarization

$$\boldsymbol{\varepsilon}_\pm = \mp\frac{(\boldsymbol{e}_x \pm \mathrm{i}\boldsymbol{e}_y)}{\sqrt{2}}.$$

We stress that a phase drift of either of the two beams is strictly equivalent to a shift of the space origin. In the following, we choose the z origin such that the relative phase ϕ is zero. For simplicity, we introduce the intensities I_+ and I_- of the σ^+ and σ^- components of the field:

$$I_\pm = I_0(1 \mp \cos 2k_L z). \tag{3.2}$$

In this formula, the spatial periodicity $\lambda_L/2$ appears clearly.

To describe in more detail the properties of the optical potential, we have to know what atomic transition to consider. We will analyse two particular cases: $J = \frac{1}{2} \to J' = \frac{3}{2}$ and $J = 4 \to J' = 5$. The first transition is the simplest case, while the second one corresponds to the most complicated transition used in experiments (caesium atom).

- Let us consider first the case of a $J = \frac{1}{2} \to J' = \frac{3}{2}$ transition: it corresponds to the original Sisyphus model [28]. The field has no π component, so that the two Zeeman sub-levels are not coupled by the field. Consequently, the Zeeman sub-levels $|g, \pm\frac{1}{2}\rangle$ remain the eigenstates of the effective Hamiltonian. The light shift has thus a simple analytical expression for each of the sub-levels (optical potential):

  $$U_\pm(z) = \tfrac{2}{3}\hbar\Delta_0'[2 \mp \cos(2k_L z)]$$

  where $\Delta_0' = \Delta s_0/2$ is the light shift per beam, and U_+ (resp. U_-) is the optical potential for the $|g, +\frac{1}{2}\rangle$ (resp. $|g, -\frac{1}{2}\rangle$) Zeeman sub-level. The minima of the potential surface U_+ coincide with the maxima of U_- and vice versa (figure 4). These extrema correspond to sites where the polarization of the total field is purely circular. For instance, a σ^+ polarization leads, for $\Delta < 0$, to a minimum for the $|g, +\frac{1}{2}\rangle$ sub-level. For $\Delta < 0$ the optical pumping accumulates the atoms at the bottom of the potential wells. The interaction with light is then maximum and the atoms scatter a lot of photons. For this reason, the red-detuned optical lattices on a $J \to J' = J + 1$ atomic transition are called bright lattices.

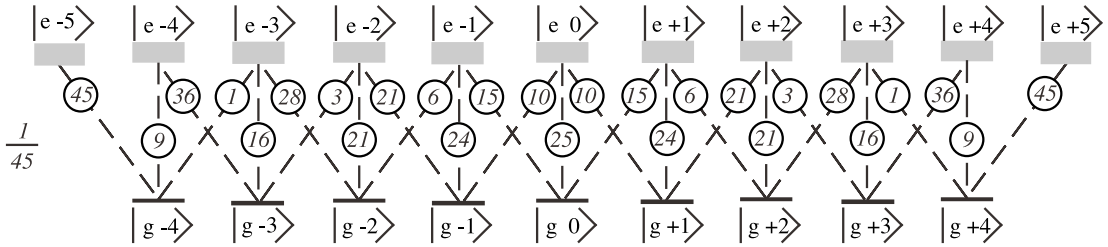

Figure 5. Squared Clebsch–Gordan coefficients in the case of a $4 \rightarrow 5$ transition. Each value must be multiplied by the common factor $\frac{1}{45}$. In the case of a $J \rightarrow J+1$ transition each Clebsch–Gordan coefficient is positive.

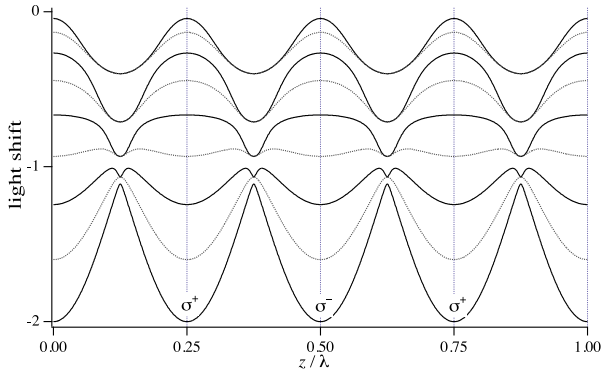

Figure 6. Adiabatic optical potential calculated in a 1D Sisyphus configuration for a $4 \rightarrow 5$ transition. Each optical potential surface can be associated with a spatially dependent eigenstate of the effective Hamiltonian. Such eigenstates are linear combinations of the Zeeman sub-levels. Two distinct families of optical potential surfaces can be identified that are not coupled by the field: the states obtained with odd Zeeman sub-levels (in grey) and the states obtained with even Zeeman sub-levels (in black). The vertical axis unit is the light shift per beam $\Delta'_0 = \Delta s_0/2$.

- For the $J = 4 \rightarrow J' = 5$ transition, actually used in caesium experiments, we have nine Zeeman sub-levels in the ground state. The Clebsch–Gordan coefficients for this transition are given in figure 5. In the absence of π-polarized light, the system splits into two parts (the odd and even m Zeeman sub-levels are not coupled by the light field). On the other hand the Zeeman sub-levels are no longer eigenstates of the effective Hamiltonian. For each position z, one has to diagonalize the atom–field interaction in order to find the potential surfaces and the nine linear combinations of the Zeeman sub-levels that give the eigenstates (figure 6). In the case of a moving atom the situation is more complex, because of the non-adiabatic transitions that can couple one potential surface to another. Nevertheless, in its steady state, this lattice is similar to the one obtained for a $\frac{1}{2} \rightarrow \frac{3}{2}$ transition: the atoms are accumulated by optical pumping cycles at the bottom of the lowest-energy potential surface. Once again, these minima correspond to positions where the polarization of the field is circular and where the scattering rate is maximum. At these points, the eigenstates are the Zeeman sub-levels and the lowest state is mainly the $m = +4$ sub-level for a σ^+ polarization. It is worth noting that the atoms are localized in an anti-ferromagnetic order, the spins in two successive wells being anti-parallel.

When the atom is localized, it goes back and forth at the bottom of the wells where the polarization of the light is circular. The potential is almost harmonic and the oscillation frequency is given by the curvature of the potential. Let us consider the σ^- site that is at the origin $z = 0$. There, the lowest level is the $|g, -4\rangle$ Zeeman sub-level. If we just follow this level close to the origin, we find its 'diabatic energy' ($\langle g, -4|H_{eff}|g, -4\rangle$) which is proportional to $I_- + \frac{1}{45} I_+$, where $\frac{1}{45}$ is the square of the Clebsch–Gordan coefficient for the $|F = 4, m = -4\rangle \rightarrow |F' = 5, m' = -3\rangle$ transition. The adiabatic potential is more difficult to evaluate; but, close to the bottom of the wells, the intensity I_+ can be treated as a perturbation [42]. In that limit, the optical potential is proportional to $I_- + \frac{1}{17} I_+$ and the maximum error made by taking this approximate formula is less than 5%†.
To evaluate the oscillation frequency, one considers the expansion of the expression (3.2) giving the intensities $I_\pm$. For the diabatic potential, the oscillation frequency Ω_v at the bottom of the wells is in the harmonic approximation:

$$\frac{\hbar\Omega_v}{E_{rec}} \simeq 2\sqrt{\frac{2\hbar\Delta'_0}{E_{rec}}\frac{44}{45}},$$

while for the adiabatic potential it becomes

$$\frac{\hbar\Omega_v}{E_{rec}} \simeq 2\sqrt{\frac{2\hbar\Delta'_0}{E_{rec}}\frac{16}{17}}.$$

It is interesting to note that the difference between the two values is about 2%, which is difficult to measure in an experiment.

3.2. Other 1D optical lattices

The simplest example of a 1D optical potential is probably the stationary wave obtained with two counter-propagating beams of the same linear polarization (lin$\|$lin configuration). In this case, the spatial intensity modulation of period $\lambda_L/2$ induces a position-dependent light shift that can affect a wide variety of atomic transitions. This configuration is often used in the far-detuned regime [9, 10] and the lattice is filled by some cooling or pre-cooling process obtained with supplementary laser beams (the field configuration itself does

† The factor $\frac{1}{17}$ is obtained for a $4 \rightarrow 5$ transition, its general expression for a $J \rightarrow J' = J+1$ transition being $1/(4J+1)$. The maximal error is obtained for $z = \lambda_L/8$ where $I_+ = I_- = I_0$. In that position, the lowest level (on a $4 \rightarrow 5$ transition) has a light shift of $\frac{10}{9}\hbar\Delta'_0$

not induce any sub-Doppler cooling). When the detuning is blue ($\Delta > 0$), the optical potential minima correspond to the nodes of the stationary wave and the atoms can be trapped in sites displaying a minimum of the photon-scattering rate [43]. As we have seen, this favourable situation can be coupled to a dissipative Sisyphus cooling process in the case of the 'grey optical lattices': atoms on a $J \to J' = J$ or $J \to J' = J - 1$ transition submitted to a longitudinal homogeneous magnetic field and to a pair of lin⊥lin blue-detuned laser beams [33, 44]. The atoms are in this case cooled and trapped in magneto-optical potential wells that are located at the minima of laser intensity. A grey lattice has been also used to design an asymmetric optical potential, allowing the observation of atomic transport in the absence of an average force [45]. Another interesting dissipative 1D optical lattice is obtained with a circularly polarized standing wave. In this situation, for $\Delta < 0$ and for a $J \to J' = J + 1$ transition, a weak transverse magnetic field can trigger a Sisyphus-like cooling that accumulates the atoms at the bottom of the most-shifted optical potential wells (magnetic assisted Sisyphus effect [46]). Finally, it is interesting to report multiple examples of 'quasi-1D' optical lattices that have been recently studied in the non-dissipative regime. These systems are obtained by crossing two beams with a Gaussian transverse profile, obtaining an interference pattern at the wavelength scale in one spatial direction and a weak dipolar confinement in the transverse direction [47,48]. In such systems a sideband cooling [47, 49–51] can be very effective in order to fill the ground state of the lattice. Such a cooling is a slight modification of the Raman cooling that selectively transfers the atoms from the excited vibrational levels to the ground state. This is possible, as we have seen, due to the energy sensitivity of the Raman pulses and to the fact that atoms are localized better than the wavelength λ_L (Lamb–Dicke regime).

3.3. Towards higher dimensions

1D optical lattices have been intensively studied from the theoretical point of view [30, 52, 53] and continue to attract a strong experimental interest, particularly in the far-detuned regime [48, 51, 54]. Obviously, the need for a generalization to higher-dimensional systems appeared very early and multiple beam configurations allowing 2D and 3D optical lattices have been introduced. We present here a study of their static properties, i.e. the optical potential and its crystallography [55]. Special attention is devoted to the role of the relative phases and the number of trapping beams.

In the particular case of a 1D Sisyphus lattice, we have seen that the spatial period of the optical potential is $\lambda_L/2$ (equation (3.2)). More generally (and in higher dimensions), the translational symmetry of an interference pattern can be determined by the wavevectors of the beams that generate it. Let us consider, for instance, the superposition of n laser beams of wavevectors $\boldsymbol{k}_j$ $(j = 1, n)$:

$$\boldsymbol{E}(\boldsymbol{r}) = \tfrac{1}{2}\mathrm{e}^{-\mathrm{i}\omega_L t}\sum_{j=1}^{n}\boldsymbol{\varepsilon}_j E_j \mathrm{e}^{\mathrm{i}\boldsymbol{k}_j\cdot\boldsymbol{r}} + \text{c.c.}$$

We can rewrite this expression giving a particular role to the first beam

$$\boldsymbol{E}(\boldsymbol{r}) = \tfrac{1}{2}\mathrm{e}^{\mathrm{i}(\boldsymbol{k}_1\cdot\boldsymbol{r}-\omega_L t)}\left(\boldsymbol{\varepsilon}_1 E_1 + \sum_{j=2}^{n}\boldsymbol{\varepsilon}_j E_j \mathrm{e}^{\mathrm{i}(\boldsymbol{k}_j-\boldsymbol{k}_1)\cdot\boldsymbol{r}}\right) + \text{c.c.} \tag{3.3}$$

Except for a global phase, we find exactly the same field $\boldsymbol{E}$ in each location $\boldsymbol{r}_{m_j}$ such that $(\boldsymbol{k}_j - \boldsymbol{k}_1)\cdot\boldsymbol{r}_{m_j} = 2m_j\pi$. This means that $\boldsymbol{K}_j = \boldsymbol{k}_{j+1} - \boldsymbol{k}_1$ $(j = 1, n-1)$ are the vectors of the reciprocal lattice, from which one can deduce the translational symmetry of the interference pattern, and consequently those of the optical lattice. If we come back to the 1D case of the field (3.1), the expression (3.3) gives us

$$\boldsymbol{K}_1 = \boldsymbol{k}_2 - \boldsymbol{k}_1 = 2\boldsymbol{k}_L,$$

which agrees with the $\lambda_L/2$ periodicity found in equation (3.2). It is interesting to note that these symmetry properties do not depend on the polarization or on the intensity of the waves.

2D optical potentials. In the 1D Sisyphus configuration, the role of the phases in the field (3.1) is easy to understand. The absolute phase is completely irrelevant, because it can vanish with the appropriate choice for the time origin. On the other hand, a change in the relative phase ϕ can be associated with a simple translation of the stationary wave along the z axis. As a consequence, the topography of the potential does not depend on the phases of the two beams. The potential is always made by a sequence of wells associated alternately with the σ^+ and σ^- polarizations of the field. In order to keep this simplicity in a 2D configuration, one has to use only three beams. In this case, the interference pattern does not depend on the phases of the beams: any phase drift of one beam results in a translation of the interference pattern in a 2D plane [56]. For three coplanar beams, it is possible to find a polarization configuration that leads to a pattern of alternating σ^+ and σ^- wells similar to the 1D lin⊥lin configuration [56]. In this lattice a dissipative Sisyphus cooling mechanism takes place and the atoms are trapped at the bottom of the potential wells.

However, the first 2D generalization of the 1D Sisyphus geometry (either experimental [57] or theoretical [58]) was obtained with four beams. The two pairs of beams in a lin∥lin standing wave configuration were in the plane with orthogonal polarizations. For a well defined value of the relative phase, the optical potential is made of the usual sequence of alternating σ^+ and σ^- wells. But for some different values of the relative phase, the polarization of light is everywhere linear, and the atoms do not accumulate any more at the bottom of the potential wells. To cope with this sensitivity to the phase, the experimentalist has to develop a special phase control loop [57].

As mentioned before, in the case of a three-beam configuration the basis of the reciprocal lattice in 2D is given by the two differences between the wavevectors of the trapping beams. The translational symmetry of the optical lattice depends only on the beams directions, but the complete crystallography of the lattice requires knowledge of the polarization and the intensity of the beams. In fact, the

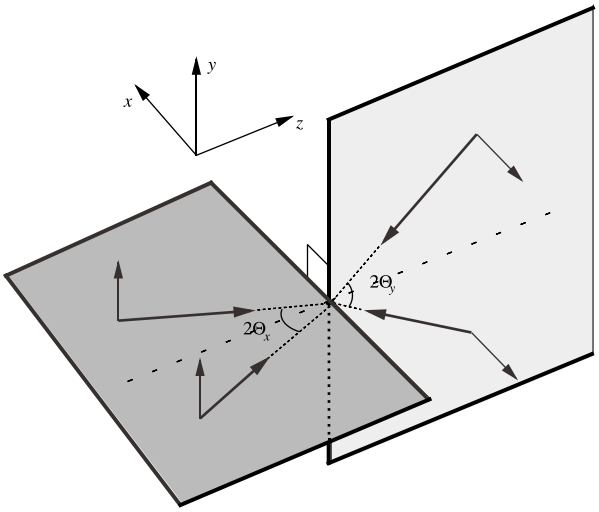

Figure 7. Trapping beam configuration in the case of a 'standard tetrahedron'. Two pairs of beams propagate on two orthogonal planes, each pair having its polarization orthogonal to the propagation plane.

decoration of the elementary cell depends on the polarization of each beam. In the case of the four-beam 2D configuration of [57], the decoration of the elementary cell depends on the relative phase, but the symmetry properties are not affected by a phase drift.

3.4. 3D optical potentials

The principle of the minimal number of beams states that, in 3D space, one has to use four non-coplanar beams in order to obtain a phase-independent topography [55, 56]. From the geometrical point of view, these 3D configurations give nothing more than the previous ones, but now the atoms are really trapped in micron-sized wells. The system is stable and the atoms can remain in the optical potential for very long times (more than 1 s). The geometry of the trapping beams gives the symmetry properties of the 3D optical lattice, as in the 1D and 2D cases. Several possibilities are described in detail in [55]. We pay special attention only to the so-called standard tetrahedron, which is probably the most studied beam configuration.

Standard tetrahedron. The beam arrangement of the 'standard tetrahedron' derives directly from the original 1D lin⊥lin configuration. Each plane wave of the 1D system is split into two waves with the same intensity in the plane orthogonal to their polarization. The waves are located symmetrically with respect to the direction of the original 1D configuration (figure 7). With the proper choice of the origin in space and time, all the relative phases can be set to zero (the topography of the lattice is phase independent). The total field thus has the following form:

$$\boldsymbol{E}_L(x,y,z) = \tfrac{1}{2}E_0 \mathrm{e}^{-\mathrm{i}\omega_L t}\sqrt{2}\mathrm{e}^{\mathrm{i}k_- z}(\varepsilon_+ E_+ + \varepsilon_- E_-) + \text{c.c.},$$

$$E_+ = \mathrm{e}^{\mathrm{i}k_+ z}\cos(k_x x) - \mathrm{e}^{-\mathrm{i}k_+ z}\cos(k_y y),$$

$$E_- = \mathrm{e}^{\mathrm{i}k_+ z}\cos(k_x x) + \mathrm{e}^{-\mathrm{i}k_+ z}\cos(k_y y),$$

where we have used the circular basis taking the z axis as the quantization axis (figure 7) and the natural notations:

$$k_x = 2\pi/\lambda_x = k_L \sin(\Theta_x)$$

$$k_y = 2\pi/\lambda_y = k_L \sin(\Theta_y)$$

$$k_\pm = 2\pi/\lambda_\pm = k_L(\cos\Theta_x \pm \cos\Theta_y)/2.$$

The symmetry properties depend on the differences of the wavevectors and, thus, on the angles Θ_x and Θ_y. In general ($\Theta_x \neq \Theta_y$), we obtain an orthorhombic lattice with the spacings λ_x, λ_y, $\lambda_+/2$. If $\Theta_x = \Theta_y$, then the lattice becomes tetragonal. For $\Theta_x = \Theta_y \simeq 63^\circ$ ($\cos\Theta_x = \cos\Theta_y = 1/\sqrt{5}$), it is face-centred cubic, and for $\Theta_x = \Theta_y \simeq 54.7^\circ$ ($cos\Theta_x = \cos\Theta_y = 1/\sqrt{3}$), it is body-centred cubic [55]. In this configuration the electromagnetic field has no π component (as in the 1D Sisyphus geometry). In the case of a $J = \frac{1}{2} \rightarrow J' = \frac{3}{2}$ transition it is easy to write the expression of the optical bi-potential:

$$U_\pm(x,y,z) = -\tfrac{8}{3}\hbar\Delta_0'[\cos^2(k_x x) + \cos^2(k_y y) \mp \cos(k_x x)\cos(k_y y)\cos(2k_+ z)].$$

Whatever the angles Θ_x and Θ_y are, the potential wells are located where the polarization of the light is circular. One is reminded of the original ID Sisyphus configuration by the structure of the wells and their alternating sequence: along the z axis, they only differ by the depth of the potential and the spacing between the minima. However, one has to keep in mind that in a 3D potential one can find some peculiar features. For instance, the total intensity is always zero along some lines parallel to the z axis and, for special directions in the xOy plane, the ellipticity of the total field remains constant. An example of an optical potential for the $4 \rightarrow 5$ transition is shown in figure 8. In this 3D case, the oscillation frequency depends on the direction of the atomic motion. In the harmonic limit for a $\frac{1}{2} \rightarrow \frac{3}{2}$ transition, the oscillation frequencies are given by

$$\frac{\hbar\Omega_{x,y}}{E_{rec}} = 4\sin\Theta_{x,y}\sqrt{\frac{\hbar\Delta_0'}{E_{rec}}}$$

and

$$\frac{\hbar\Omega_z}{E_{rec}} = 4(\cos\Theta_x + \cos\Theta_y)\sqrt{\frac{\hbar\Delta_0'}{3E_{rec}}}.$$

For a $4 \rightarrow 5$ transition, the frequencies along the x and y directions do not change. The only difference is found for the z frequency, which is now equal to

$$\frac{\hbar\Omega_z}{E_{rec}} = 4\frac{\cos\Theta_x + \cos\Theta_y}{\sqrt{2}}\sqrt{\frac{16\hbar\Delta_0'}{17E_{rec}}}.$$

It is interesting to note that, for the regular tetrahedron, the frequencies are almost degenerate for the $4 \rightarrow 5$ transition ($\Omega_z = \sqrt{\frac{16}{17}}\Omega_{x,y}$), while they are quite different for a $\frac{1}{2} \rightarrow \frac{3}{2}$ transition.

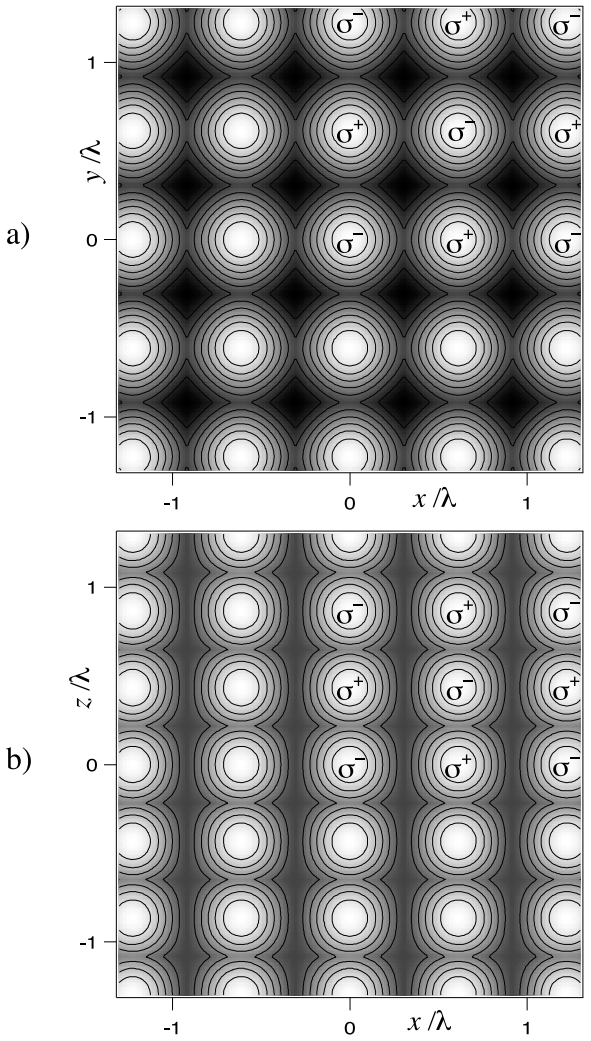

Figure 8. Optical potential sections in (*a*) the xy plane and (*b*) the xz plane obtained with a 'standard tetrahedron' beam configuration in the case of a $4 \rightarrow 5$ transition (most shifted adiabatic potential surface). Optical potential minima (white regions in the figures) correspond to circular polarization sites. The alternating sequence of σ^+ and σ^- sites induces an anti-ferromagnetic orientation in the atomic sample. This particular optical potential is obtained for $\Theta_x = \Theta_y = 54.7^\circ$ (regular tetrahedron).

Optical super-lattices and quasicrystals. As we have seen, the translational symmetry properties of an interference pattern obtained with n beams are determined by the $n-1$ reciprocal lattice vectors $\boldsymbol{K}_j = \boldsymbol{k}_{j+1} - \boldsymbol{k}_1$ ($j = 1, n-1$). In the case of a four-beam configuration ($n = 4$), three vectors span the physical 3D space; what happens if more than four beams are used to create an optical potential? From a mathematical point of view the answer is quite simple: the reciprocal vectors will generally span a $(n-1)$-dimensional space. The optical potential that affects the atomic motion in the physical space is obtained by a geometrical 3D cut of this mathematical space [59], exactly as in the case of solid-state structures [60]. The use of 'redundant-beam configurations' therefore allows the tailoring of optical potentials and the creation of structures already observed in solid-state systems. A first example of these systems is the optical super-lattice [61]. This system is obtained by adding to a (periodic)

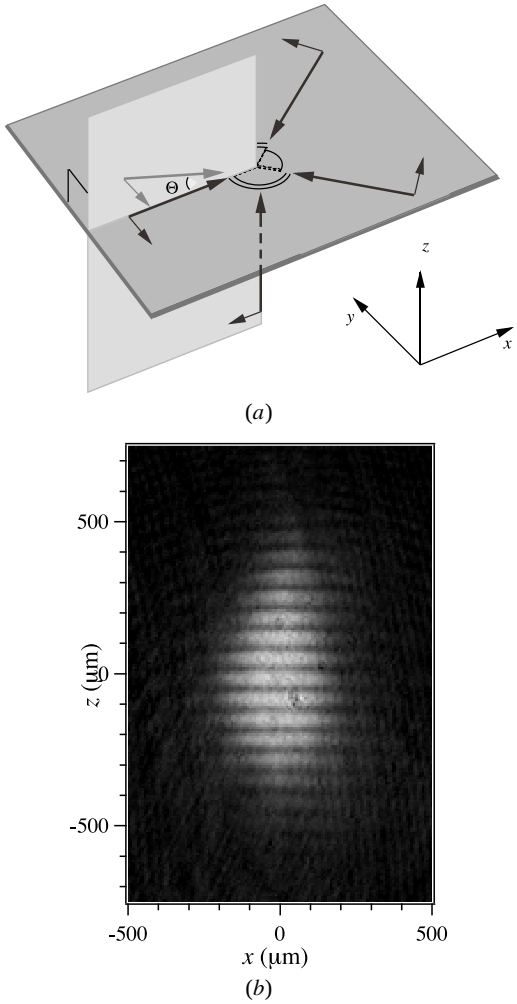

Figure 9. (*a*) Five-beam configuration of the Sisyphus optical super-lattice. All the beams are polarized in the xy plane and the angle Θ between the fifth beam and the plane is very small (tens of milliradians). (*b*) Shadow image of an optical super-lattice. The resonant 'flash' beam is turned on during 100 μs with an intensity of 100 μW cm^{-2}. The trapping beams are turned off before the image recording; a background image obtained without cold atoms has been subtracted (see section 5.4).

four-beam configuration a fifth beam that introduces a very short vector in the reciprocal space (small angle between two beams: see figure 9(*a*)). In this situation, a long-range modulation along the z direction is superimposed to the λ_L-spaced optical potential wells, allowing a direct observation of the atomic density distribution (see figure 9(*b*)).

Another important feature that can be obtained with redundant-beam configurations is the loss of translational symmetry of the optical potential [62]. For instance, a 2D optical potential with a fivefold symmetry can be obtained just by aligning five trapping beams along the axis of a regular pentagon. The 'optical quasicrystals' obtained in this way share with their solid-state analogue [63] the intriguing physical properties induced by a perfectly ordered potential in absence of translational symmetry.

Holographic optical lattices. A completely different strategy to obtain optical lattices was introduced in [64].

If a plane wave passes through a phase object (for example, a holographic grating) it is possible to obtain an electromagnetic field that displays strong spatial intensity and/or phase modulations. This field induces a position-dependent light shift that can be used to trap cold atoms in the far-detuned regime [64]. The spatial symmetry properties of the optical lattice are, in this case, entirely determined by the design of the phase object. The transverse modulation is induced by the hologram plate and a longitudinal modulation is also present, due to the Talbot effect (present in the intermediate-field diffraction region). These phase objects have been also used in the dissipative regime in order to induce a 3D polarization-gradient cooling. In this case, the diffracted light interferes with a counter-propagating plane wave with an orthogonal linear polarization (3D Sisyphus–Talbot optical lattice [65]).

The phase object can display a random spatial distribution instead of a periodic structure. In this case, the electromagnetic field will present a random phase and intensity distribution. The possibility of cooling and trapping the atoms in such disordered optical lattices has been proved in theory [66] and in an experiment [67]. These systems can therefore be considered as the atomic analogue of solid-state glasses.

4. Theoretical approaches and numerical simulations

In this section, we briefly present the main theoretical approaches that have been used to solve the problem of the motion of an atom (with several Zeeman sub-levels) in an electromagnetic field $\boldsymbol{E}_L(\boldsymbol{r},t)$ due to the interference of several laser beams with the same frequency ω_L. All the approaches start from the generalized optical Bloch equations that describe the evolution of the atomic density matrix. These equations are obtained by considering the field as a classical field and the atom–field interaction in the rotating wave approximation. The vacuum is considered as a quantum reservoir and it is responsible for the relaxation phenomena (spontaneous emission).

The whole problem cannot be solved analytically, even in the simplest cases. Different approaches have been developed, depending on the approximations that can be made. Numerical evaluations are very often used. Here we present briefly the different approaches and we try to stress the advantages and the weaknesses of each.

4.1. Optical pumping equation

As mentioned earlier, the starting point for the study of the atomic motion is given by the generalized optical Bloch equations. In the limit of weak saturation, large detunings and small velocity, we can adiabatically eliminate the excited states, leading to the optical pumping equation [39, 68]:

$$\frac{\mathrm{d}\sigma}{\mathrm{d}t} = \frac{1}{\mathrm{i}\overline{h}}[H_{eff},\sigma] + \left(\frac{\mathrm{d}\sigma}{\mathrm{d}t}\right)_{relax}. \tag{4.1}$$

This equation describes the time evolution of the density matrix σ reduced to the ground state. It is a square matrix whose dimension is given by the number of Zeeman sub-levels in the ground state. The diagonal terms σ_{ii} are the populations of the sub-levels, while the off-diagonal terms $\sigma_{ij} = \sigma_{ji}^*$ represent the Zeeman coherences induced by the electromagnetic field. The equation (4.1) is naturally split in two parts.

- The first part, which is called reactive, describes the Hamiltonian motion and contains the effective Hamiltonian:

$$H_{eff} = \frac{|\boldsymbol{P}|^2}{2M} + \Lambda(\boldsymbol{R}), \tag{4.2}$$

  where $\boldsymbol{P}$ and $\boldsymbol{R}$ are the momentum and position (vectorial) operators. The $\Lambda(\boldsymbol{r})$ operator is called the light-shift operator and describes the spatial dependence of the optical potentials. This operator depends on the amplitude $E_L(\boldsymbol{r})$ and local polarization $\varepsilon_L(\boldsymbol{r})$ of the field, on the detuning Δ, and on the natural line-width Γ. Its expression is given by (s being the previously introduced saturation parameter)

$$\Lambda(\boldsymbol{r}) = \overline{h}\frac{\Delta s(\boldsymbol{r})}{2}A(\boldsymbol{r}),$$

  with

$$A(\boldsymbol{r}) = [\boldsymbol{d}^- \cdot \varepsilon_L^*(\boldsymbol{r})][\boldsymbol{d}^+ \cdot \varepsilon_L(\boldsymbol{r})]. \tag{4.3}$$

  In the circular basis

$$\varepsilon_{\pm1} = \mp\frac{(\boldsymbol{e}_x \pm \mathrm{i}\boldsymbol{e}_y)}{\sqrt{2}}$$
$$\varepsilon_0 = \boldsymbol{e}_z$$

  the matrix elements of the reduced dipole operator $d_q^{\pm} = \varepsilon_q \cdot \boldsymbol{d}^{\pm}$ ($q = 0, \pm1$), introduced in equation (4.3), are given by the Clebsch–Gordan coefficients of the considered transition.

  The quantity $\overline{h}\Delta' = \overline{h}\Delta s/2$ is the light shift of the ground state $|g\rangle$ of a two-level atom in the total field of amplitude E_L (equation (2.2)). This quantity gives the order of magnitude of the optical potential energy, except for the fine dependence on the geometry and the local polarization of the field, that is contained in the operator A. The eigenvectors of the light-shift operator are, in general, linear combinations of the Zeeman sub-levels that depend on the point $\boldsymbol{r}$. The associated eigenvalues define the various optical potential surfaces. It is important to note that the kinetic energy term in equation (4.2) does not commute with Λ. It is thus not possible to separate the effective Hamiltonian without an extra simplifying hypothesis.
- The second (dissipative) part takes into account the relaxation processes:

$$\left(\frac{\mathrm{d}\sigma}{\mathrm{d}t}\right)_{relax} = -\frac{\Gamma'}{2}\{A(\boldsymbol{r}),\sigma\} + \frac{3\Gamma'}{8\pi}\int \mathrm{d}^2\Omega_{\boldsymbol{\kappa}} \sum_{\epsilon\perp\boldsymbol{\kappa}} B_{\epsilon}^{\dagger}(\boldsymbol{r})\mathrm{e}^{-\mathrm{i}\boldsymbol{\kappa}\cdot\boldsymbol{r}}\sigma\,\mathrm{e}^{\mathrm{i}\boldsymbol{\kappa}\cdot\boldsymbol{r}}B_{\epsilon}(\boldsymbol{r}), \tag{4.4}$$

  where $\Gamma' = \Gamma'(\boldsymbol{r}) = \Gamma s(\boldsymbol{r})/2$ is the photon scattering rate. It gives the characteristic time scale for the optical pumping processes considered in this dissipative part of equation (4.1). The second term in equation (4.4) describes the emission of a spontaneous photon with the wavevector $\boldsymbol{\kappa}$ and the polarization $\boldsymbol{\epsilon}$ in the solid angle $\mathrm{d}^2\Omega$ by the operator B_{ϵ}.

4.2. Resolution of the optical pumping equation

The optical pumping (equation (4.1)) is very complex and several approximations have been introduced in order to solve it. The $\frac{1}{2} \rightarrow \frac{3}{2}$ transition is the most widely studied because of its simplicity: in the absence of π-polarized light, the Zeeman coherences vanish. The study of more complex transitions is motivated by the comparison with the experiments that are commonly done on the $2 \rightarrow 3$, $3 \rightarrow 4$ or $4 \rightarrow 5$ transitions.

Elimination of the internal degrees of freedom. This method, introduced in [28], derives from the description of the Doppler cooling. It consists of the adiabatic elimination of the internal degrees of freedom of the atom. The cooling process is then described by a Fokker–Planck equation where the external degrees of freedom are treated classically. The effects of the light shift and of the optical pumping are summarized in a friction force and a momentum diffusion coefficient. It is then possible to evaluate the stationary density and distribution in momentum space. This type of approach has been used to estimate the temperatures in optical molasses [69, 70], and to study the diffusion phenomena in 2D optical lattices [71, 72]. Unfortunately, this approach is not valid when the atoms are localized in a wavelength-scale potential well. This method is not able to predict the 'décrochage' that is observed for low laser intensities. In this particular case a quantum description of the atom is important.

Direct integration. To solve the complete problem given by equation (4.1), one can try to evaluate the evolution of the density matrix σ. However, in numerical studies, it is necessary to sample the momentum distribution. Such a discretization is often done in the limit of low intensities, where the stationary momentum distributions are not too wide; nevertheless, the number of density matrix elements quickly becomes very big. Even taking into account all the symmetries of the field and considering a simplified spontaneous emission diagram (which allows bins with a dimension $\overline{h}k_L$ in momentum space), the limiting factor is the size of the matrices. For instance, for a 2D Sisyphus optical lattice on a $\frac{1}{2} \rightarrow \frac{3}{2}$ transition [58], one has to manipulate 300 000 matrix elements. Even if the direct integration method does not introduce any approximation, it is extremely computing-time consuming. An extension of this method to a 3D problem seems almost impossible.

Band method. The band method, introduced in [30] for a $\frac{1}{2} \rightarrow \frac{3}{2}$ transition in a 1D configuration, takes advantage of the translational symmetry of the optical lattice. As in the case of electrons in a solid-state lattice, the atomic wavefunction must satisfy the Bloch theorem. One then uses the Bloch state basis to rewrite the optical pumping equation (4.1). In the secular limit, where one can neglect the coherence between two different bands, one deduces from equation (4.1) a rate equation for the populations of the various bands. This approximation treats perturbatively the effect of the relaxation term (4.4) and is valid in the oscillating regime: the atom goes back and forth several times in the potential well between two successive optical pumping processes. The band method gives a completely quantum description of the problem and has been used in the case of complex transitions [73] to study the dynamical properties [52] and the magnetism of the optical lattices [74]. More recently, a slightly modified version of the band method that uses the Wannier states instead of the Bloch states has been developed to investigate the local cooling phenomenon [75] as well as the quantum state preparation in the far-detuned regime [76]. All the preceding examples deal with 1D optical lattices. In fact, the secular approximation is, already in 1D, limited to the regime of very large detunings. In higher dimensions, the degeneracy of the bands increases and the validity domain of these calculations is dramatically reduced. Nevertheless, the band method has been used to study the 2D optical lattices in a three-beam [77] and in a four-beam [58] configuration.

Quantum Monte Carlo simulation. The quantum Monte Carlo method [78, 79] has been introduced in quantum optics to treat dissipative phenomena without solving the master equation, which is expensive from the point of view of computing time. The basic idea is simple: one follows many times the evolution of a single wavefunction of the system in order to obtain a statistical ensemble of wavefunctions. The information about the mean value of a given operator is obtained by taking the average on this statistical ensemble. The evolution of each wavefunction is obtained by considering Hamiltonian evolution periods (calculated with a non-Hermitian Hamiltonian) followed by quantum jumps that occur when a spontaneous photon is emitted. This method, associated with the band description of the wavefunctions described in the preceding paragraph, has been successfully used to study the temperature and fluorescence spectra of 1D optical lattices [53, 80, 81]. A wavefunction simulation has been also used to reproduce the dependence of the temperature as a function of the light shift in the case of 3D optical molasses [82]. This dependence is in good agreement with the experimental results obtained for $2 \rightarrow 3$, $3 \rightarrow 4$ and $4 \rightarrow 5$ transitions. More recently, this method has also been used to study the anomalous diffusion, the magnetic properties and the wavepacket dynamics in 1D optical lattices [72, 83, 84]. Moreover, the case of optical super-lattices has been also studied by a wavefunction simulation based on the band method [85].

The main advantage of the quantum Monte Carlo simulation is that it allows the quantum treatment of any atomic transition without approximation. This kind of simulation can also give 3D density and momentum distributions [82], but the cases of 2D and 3D optical lattices have not been studied yet. The computing power required limits in fact the use of this method in 2D and 3D. On the other hand, it is difficult to have a simple physical image of the processes that lead the system to its steady state.

Semi-classical Monte Carlo simulation. The semi-classical Monte Carlo simulation, introduced in [58], keeps the internal structure of the atom, but describes the external degrees of freedom classically. In particular, one uses a series development of the Wigner representation of the

density matrix σ up to the second order in $\hbar k_L/\bar{p}$ (where $\bar{p}$ is the characteristic width of the momentum distribution). This approximation is thus valid only if the momentum distribution is not too narrow, which is equivalent to the limit of a spatially localized atomic wavefunction. This kind of simulation is very useful in the case of a $\frac{1}{2} \rightarrow \frac{3}{2}$ transition in a field configuration without a π-polarized component. In this case, equation (4.1) can be rewritten into two Fokker–Planck equations coupled by the optical pumping processes. These equations describe the evolution of a Brownian classical particle in a bi-potential (the optical potential). The particle changes its internal state with a rate given by the optical pumping rate, and is also driven by the radiation pressure force. A momentum diffusion coefficient accounts for the recoil effects during the spontaneous emission processes. This kind of simulation has been used to study 1D and 2D optical lattices [58, 86, 87] and, more recently, 3D lattices in the case of a $\frac{1}{2} \rightarrow \frac{3}{2}$ transition [88]. A 1D generalization to higher J has been made [89], but its validity is limited by the adiabatic following hypothesis that is made to neglect the Zeeman coherences. The main advantage of the semi-classical Monte Carlo simulation is its simplicity. The underlying physical processes are clearly visible and it is easy to control the individual effects of each of them. The limitation of this semi-classical method comes from the difficulty of describing transitions with higher J in 2D or 3D. For instance, it is difficult to take into account the local cooling mechanism that may be dominant in optical lattices [75, 83].

5. Optical lattice characterization

In this section, we present a short review of the methods that give information about the atomic motion in an optical lattice. For example, we will show how the analysis of the atomic fluorescence can give information about the localization and the diffusion of atoms in the lattice [41, 90, 91]. Several of the techniques presented here are commonly used as diagnostics in other laser cooling schemes, but some of them (e.g. Bragg diffraction, which relies on the long-range order) are characteristic of optical lattices. All the diagnostic methods share two common points: they have to be simple enough to be implemented in the experiments and they must have an immediate theoretical interpretation.

5.1. Pump–probe spectroscopy

Pump–probe spectroscopy of laser-cooled atoms was introduced in 1991 [92], and subsequently led to the first observation of the oscillation of the atoms trapped in the potential wells of a 1D optical lattice [40, 52]. This technique is flexible and allows a detailed investigation of the atomic dynamics in these structures. The method relies on the idea, commonly used in nonlinear optics [93], that the simultaneous interaction of the sample with an intense pump beam of frequency ω_{Pump} and a weak probe beam of frequency ω_{probe} gives information about the dynamical modes at the frequency of the beat note $\delta_{Pp} = \omega_{Pump} - \omega_{probe}$. One can either study the transmission of the probe, or look for four-wave mixing as a function of δ_{Pp}. In the particular case

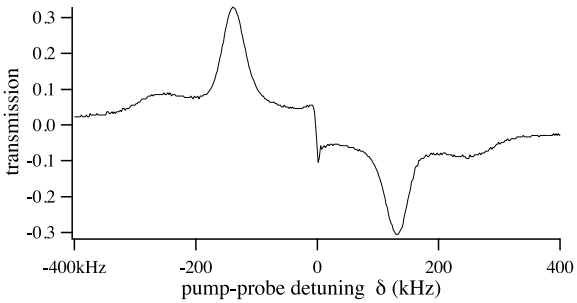

Figure 10. Experimental transmission spectrum obtained by scanning the probe frequency ω_{probe} around the trapping-beam frequency ω_L in a 'standard tetrahedron' optical lattice. Experimental conditions: $\Theta_x = \Theta_y = 55 \pm 1^\circ$, Intensity per beam $I_0 = 17$ mW cm^{-2}, probe intensity $I_{probe} = 110$ μW cm^{-2}, probe direction $\boldsymbol{e}_x + \boldsymbol{e}_y$, probe polarization in the xy plane.

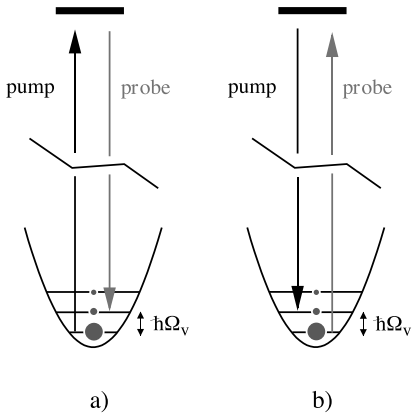

Figure 11. Raman processes at the origin of the most important peaks in the transmission spectrum of an optical lattice. (*a*) When $\delta = -\Omega_v$, the dominant contribution (due to 'thermal' population difference) is the pump-photon absorption preceding a probe-photon emission (net gain on the probe). (*b*) When $\delta = \Omega_v$, the probe is preferentially absorbed.

of laser-cooled atoms, the trapping beams are always present and can be considered as the pump beams. Thus, it is only necessary to add a probe beam characterized by its detuning $\delta = \omega_L - \omega_{probe}$ with respect to the trapping beams.

Transmission spectroscopy. This method consists of measuring the transmitted intensity of the probe beam while scanning the detuning δ. It has been used to study the 1D Sisyphus lattices [40, 94] and their 2D [56, 57] and 3D [56, 95, 96] generalizations. Its theoretical interpretation has been given in 1D [52] and 2D [97]. An example of an experimental transmission spectrum, obtained in a standard tetrahedron, is given in figure 10. The details of this kind of spectrum depend on the geometry of the lattice, the propagation direction of the probe, and its polarization. However, we can take this spectrum as an example, describe its features and give their interpretation.

- The two peaks, on each side of the degeneracy and with opposite signs (gain for $\delta < 0$ and absorption for $\delta > 0$) are due to Raman transitions between the vibrational levels of the atom trapped in a potential well. As already mentioned, the quantum description

of the Sisyphus cooling predicts a band structure for the atomic external degrees of freedom [30]. Pump–probe spectroscopy allows the direct observation of this structure with two-photon transitions. These transitions are resonant when the pump–probe detuning δ coincides with the difference in energy between the bands, some selection rules limiting the possible couplings. The sign is also explained by the theory: it is related to the fact that the lower bands have the higher populations (figure 11). The width of the Raman lines is much smaller than the photon scattering rate. This surprising effect is due to the fact that a spontaneous photon does not destroy a coherence between the bands. In the semi-classical point of view, it means that the phase of the atomic oscillation at the bottom of the potential wells survives the recoil in an optical pumping cycle. This phenomenon is related to the strong localization of the atom in the sub-wavelength potential wells (Lamb–Dicke narrowing).

- The narrow feature in the centre of the spectrum is a Rayleigh-type resonance. Its interpretation is given in terms of two-wave mixing that has been already observed in the usual 'hot' atomic vapours [98]. A detailed description of this resonance in the case of optical lattices is given in [52]. Here we just report an example from among the wide variety of physical processes eventually leading to this kind of resonance. When a probe is added to the system, it introduces a small modulation of the properties of the lattice: for instance, a change in the depth of the potential wells. This modulation is completely static when the detuning δ is zero, otherwise it moves with a velocity that is proportional to δ. In the static case, the atoms are simply redistributed in the new potential, reaching a new 'equilibrium' where the deepest wells are the most populated. In this way we obtain an atomic modulation that reproduces the intensity pattern without any dephasing. For symmetry reasons in this situation no power transfer is possible between pump and probe: the density grating has no way of choosing if it should transfer photons from the pump into the probe direction or vice versa. On the other hand, in the presence of a small detuning δ we have a drift of the interference pattern, and the atomic density tries to follow this drift. However, the response time of the atomic density being finite, the density modulation becomes phase shifted with respect to the intensity pattern. In this moving case, an energy transfer between the pump and the probe (or vice versa) becomes possible, because of the interference phenomenon between the probe and the partially diffracted pump that is no longer in quadrature. Depending on the sign of the phase shift, the interference is constructive or destructive. For detunings δ much larger than the characteristic response time, the atoms no longer follow the intensity modulation and no density grating is created. The shape of the Rayleigh resonance is then dispersive, with a width that depends on the spatial diffusion characteristic time.

These spectral features are not the only ones that can be observed. For instance, new peaks can appear in the spectrum obtained in the standard tetrahedron with small angle: 'Brillouin' resonances [86, 99]. These resonances are associated with a propagating mode in the optical lattice and are excited when the drift velocity of the pump–probe interference pattern coincides with a characteristic velocity that depends only on the depth of the wells and their geometry. Finally, some Raman transitions between the potential surfaces associated with the different Zeeman sub-levels (figure 6) can be observed for a properly chosen polarization of the probe.

From the theoretical point of view, one evaluates the transmission spectra introducing the probe field in the total field. Using either the quantum method in 1D [52], or the semi-classical approach in 2D [97], one can calculate the mean energy transfer between the pump and the probe. From the experimental point of view, this method is simple to implement, and gives spectra with a good signal-to-noise ratios without requiring long acquisition times. The only point that one has to control properly is the stability of the beat note δ, as the narrower structures may be sub-kHz. Usually, pump and probe come from the same laser source and are frequency shifted by acousto-optic modulators. The required stability is then easily obtained using RF synthesizers.

Coherent transient. The coherent transient method is an extension of the pump–probe spectroscopy method, introduced in 1993 [95] and developed later [100]. As in the previous case, a weak probe beam is added to the optical lattice in order to excite its dynamical modes, but, now, in a first excitation phase the probe frequency remains fixed until a steady state is obtained. For instance, if we choose $\delta = \Omega_v$ we will excite the oscillation of the atoms in the wells (or, quantum mechanically, create Raman coherences between the vibrational levels). Once the 'equilibrium' is reached, the frequency of the probe is shifted abruptly (quicker than all the relevant characteristic times) to a new value such that no dynamical mode can be excited. In this new configuration the lattice relaxes to an equilibrium which is almost the unperturbed one (in the absence of the probe beam). During this relaxation phase, the pump beams are still diffracted in the probe direction, due to the presence of the dynamical mode previously excited. This diffracted light is easily measured by heterodyne detection with the probe beam at its new frequency. The information on the dynamics of the atoms in the lattice is contained in the envelope of the beat signal. A simple Fourier transform relation can be demonstrated between the usual pump–probe frequency spectra and time-resolved coherent transients. Such a relation is valid only in the linear regime where the probe is weak. For stronger probes, the transmission spectra are hardly sensitive to the saturation, while, in contrast, the coherent transients exhibit a strong selective saturation [42]. For the experimentalist, the coherent transient method is relatively simple to implement and, in some conditions, it allows an increase of the signal-to-noise ratio by a factor of ten. The main difficulty comes from the frequency jump, which is of the order of 1 MHz, and must preserve the relative pump–probe phase if we want to average the transient signal.

Four-wave mixing. Four-wave mixing is a nonlinear process that can be observed with pump–probe spectroscopy. This process involves four photons (two are absorbed and

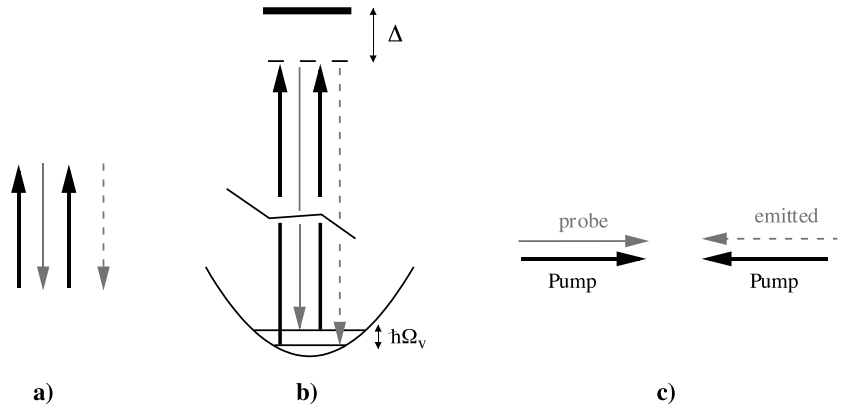

Figure 12. Phase-conjugation phenomena in a 1D optical lattice. (*a*) Picture of the absorption–emission processes for the four photons: a pump-photon absorption (black) precedes a stimulated emission of a probe photon (grey), followed by the absorption of a new pump photon. The conjugated wave is represented by a dotted arrow. (*b*) Energy conservation in vibrational transitions: the whole process is resonant for $\delta = \omega_L - \omega_{probe} = \pm\Omega_v$, which means $\omega_c - \omega_{probe} = 2\delta$. (*c*) Momentum conservation in the 1D case: the conjugated wave propagates in the opposite direction with respect to the probe.

two others emitted) and preserves the total energy and momentum. The phase-matching condition, which is nothing else but momentum conservation, leads to the coherent amplification of a wave, in a particular direction and with a precise frequency. In optical lattices, two different four-wave mixing processes have been observed: phase conjugation and elastic coherent diffusion. These two processes differ according to the nature of the emitted photon.

- In the case of phase conjugation, the two absorbed photons are pump photons, and the emission of a stimulated photon in the probe occurs. As a consequence, a wave at the frequency $\omega_c = 2\omega_L - \omega_{probe}$ is emitted. In a 1D lattice [94], this wave travels in the direction opposite to the probe, and its amplitude is the complex conjugate of that of the probe. The process is due to the polarization induced by the absorption of a pump photon, immediately followed by the emission of a probe photon and the absorption of a photon in the other pump beam. The wavevector $\boldsymbol{k}_c$ of this induced polarization is

$$\boldsymbol{k}_c = \boldsymbol{k}_{L,1} - \boldsymbol{k}_{probe} + \boldsymbol{k}_{L,2} = -\boldsymbol{k}_{probe},$$

  because $\boldsymbol{k}_{L,1} = -\boldsymbol{k}_{L,2}$ (figure 12). It is possible to record simultaneously the transmission spectrum and the four-wave mixing spectrum. The two spectra present features for the same detunings $\delta = 0, \pm\Omega_v$ for which the underlying process is resonant.
- The case of elastic coherent diffusion differs from the previous one because the probe photon is now absorbed and a pump photon is emitted. The phase-matching condition now reads $\boldsymbol{k}_{L,i} - \boldsymbol{k}_{L,j} = \boldsymbol{k}_{probe} - \boldsymbol{k}_c$. This condition is equivalent to the Bragg condition in the case of optical lattices [56]. For instance, a probe that travels in the direction opposite to a pump beam will generate an elastic diffusion wave in the directions opposite to each of the pump beams. Two different processes occur, that differ according to the order in which the photons are absorbed or emitted (figure 13). The atoms can first absorb a probe photon or a pump photon. In the first case, the process is resonant when $\delta = 0, \pm\Omega_v$: a Raman transition between vibrational levels is observed. In the second case, which is equivalent to Bragg diffraction when the atomic density is the created observable, the intermediate step is always resonant.

Figure 13. Elastic coherent diffusion: illustration of the absorption–emission of the four photons involved in the two kind of processes. (*a*) A pump beam is diffracted by an observable that has been previously induced by the absorption of a probe photon (in grey), followed by the stimulated emission of a pump photon (in black). (*b*) Bragg diffraction: the probe is diffracted by an observable previously induced by an absorption-stimulated emission of two pump photons.

Photon redistribution measurements. The reactive force described by the Hamiltonian (4.2) has its origin in repeated coherent cycles of absorption and stimulated emission. During these cycles, photons are redistributed among the trapping beams allowing a net momentum transfer to the atom. This process can be viewed as a pump–probe phenomenon in which the trapping beams play both the roles of the pump and of the probe. In the case of an unperturbed 'thermal' optical lattice, the average power transfer between the trapping beams vanishes, because there is no preferential direction for the confining forces. However, if the initial position and/or momentum distributions of the atoms submitted to the optical potential are not symmetric, a temporal evolution of the trapping beam intensity is expected, reflecting the changes of the average direction of the force imposed on the atomic sample by the trapping beams. This principle has been used to explore the atomic wavepacket dynamics in optical lattices simply by monitoring the time evolution of the intensity of the trapping beams.

The initial asymmetry can be produced in two ways. In the first method, an abrupt phase shift (obtained with a liquid-crystal phase modulator) in a lattice beam induces a sudden translation of the optical potential. The position distribution is shifted with respect to the bottom of the potential wells and the average force direction starts to oscillate following the oscillations of the wavepackets in the potential wells [84]. In another experiment, a moving 1D optical potential (obtained with a slight ($\simeq$10 kHz) frequency shift between the two trapping beams) is loaded with a static cloud of cold atoms. In the moving frame associated with the lattice, the momentum distribution does not average to zero; with such an initial condition all the atoms oscillate in phase back and forth in the optical potential and the average reactive force periodically changes its direction [101].

This technique allowed the study of the wavepacket dynamics in optical lattices, including the direct measurement of the damping of atomic oscillation (mainly due to the anharmonicity of the optical potential [101–103] and the observation of collapses and revivals in the atomic dynamics [84]. From an experimental point of view, the technique is relatively simple to implement and the signal-to-noise ratio is high, as in the case of stimulated processes. The results can be quantitatively interpreted with a quantum wavefunction simulation, either using a direct relationship between the calculated average force and the power redistribution [84] or in the frame of the recoil-induced resonance [101, 104].

5.2. Fluorescence analysis

The spectral analysis of the fluorescence emitted by the cold atoms is the first method that demonstrated a Lamb–Dicke narrowing due to the localization of the atoms at the wavelength scale [105]. To achieve the required resolution, a heterodyne technique, with a local oscillator derived from the trapping laser, is necessary. Experiments analysing the frequency spectrum of the emitted fluorescence were performed in 1992 for the 1D optical lattices [41] and in 1997 for the 3D standard tetrahedron [106]. An extension of this method, investigating the intensity correlations of the scattered photons, was developed to study the diffusion properties in a 3D optical lattice [90, 99]. Finally, a temporal study of the fluorescence allowed the demonstration of breathing motion of the atoms in time-modulated 3D optical potential wells [91].

Fluorescence spectrum. The frequency analysis of the fluorescence of a 1D optical lattice permits the observation of the sidebands due to the oscillatory motion of the atoms in the potential wells [41]. More precisely, the fluorescence is emitted mainly in a narrow peak corresponding to elastic diffusion (the width of this peak is a few kHz, and is attributed to the vibration of the mirrors), but two smaller contributions, symmetric on each side of the pump frequency, show up. The distance between these sidebands and the central peak coincides with the vibration frequency Ω_v of the atom at the bottom of the potential well. These sidebands are due to the spontaneous Raman transitions between vibrational levels in the optical lattice. The absorption of a pump photon can be followed by the emission of a more or less energetic photon

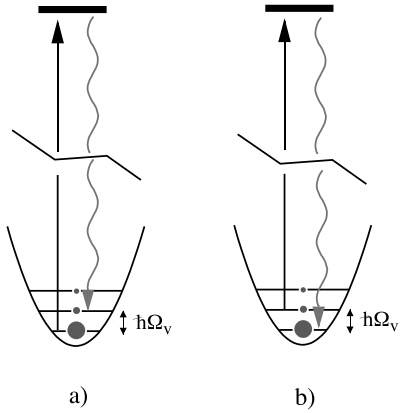

Figure 14. Spontaneous Raman processes in an optical lattice. (*a*) Raman Stokes spontaneous transition: the atom absorbs a photon in a trapping beam, and emits a spontaneous photon which raises it to a more energetic band. (*b*) Raman anti-Stokes transition: the emitted photon is more energetic than the trapping photons.

that brings the atoms back to the ground state but at another vibrational level (figure 14). The ratio of the energy contained in the sidebands to that of the elastic diffusion is very small. This result demonstrates that the atoms are localized on a scale smaller than the optical wavelength (Lamb–Dicke narrowing). Moreover the difference in intensity of the Raman Stokes and anti-Stokes peaks gives information on the population differences between vibrational levels. As in the case of pump–probe spectroscopy, the choice of the observation direction allows the discrimination of the oscillation frequencies associated with the different spatial directions [106].

From a theoretical point of view, the evaluation of the emitted fluorescence in 1D optical lattices is performed either by semi-classical methods or with wavefunction Monte Carlo simulations [53, 80]. Experimentally, this approach has the disadvantage of all the methods which detect spontaneous processes: the signal is weak and long acquisition times (of the order of the hour) are required to achieve a good signal-to-noise ratio.

Intensity correlations. The study of the temporal correlations displayed by fluorescence intensity is closely related to the spectral analysis of the fluorescence. This method has been applied to a 'standard tetrahedron' Sisyphus optical lattice in order to study both the self-correlation of photons with the same polarization, and the cross-correlation between photons of orthogonal polarization. In the first case, the collected information does not differ from the information obtained with the spectral analysis of the fluorescence. More precisely, the Wiener–Khintchine theorem gives a simple relation by Fourier transform between the two signals. On the other hand, the cross-correlations give information about the characteristic time that is needed to jump from one potential well to another. If the motion is diffusive, one can deduce from this time a diffusion coefficient. The experimental value of this diffusion coefficient [90] is much lower than the one found in optical molasses [71].

From the theoretical point of view, this method has been analysed with semi-classical Monte Carlo simulations, in 1D

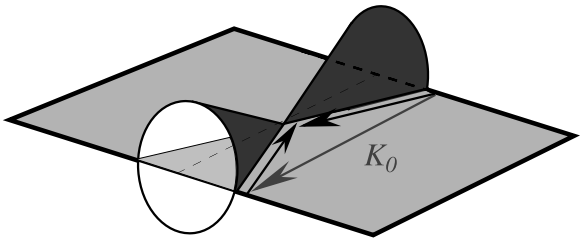

Figure 15. Bragg diffraction in optical lattices. The Bragg condition associates a cone to each reciprocal-lattice vector $\boldsymbol{K}_0$. In order to have Bragg diffraction, the incoming and diffracted beam wavevectors must lie on one of these cones. In particular, a couple of trapping beams is always on a 'Bragg cone'.

and 2D [90, 99]. To evaluate the correlation function, one estimates the time interval between two emission processes, with a classical average over an ensemble of trajectories. The experimental investigation of intensity correlations shares, with the spectral analysis of the fluorescence, the long acquisition times needed to reach a good signal-to-noise ratio.

5.3. Bragg diffraction

Bragg diffraction in optical lattices demonstrates the presence of a long-range order in these structures [62, 107, 108]: as in solid crystals, the atomic density in optical lattices displays a coherent spatial modulation. In solids, the periodicity is of the order of 0.1 nm, and is given by the self-arrangement of the ions in the lattice. For optical lattices, the modulation is related to the interference pattern of the trapping beams, and its characteristic length scale is a fraction of the wavelength $\lambda_L \simeq 1\mu$m. Bragg diffraction relies on a constructive interference of the light scattered by successive crystallographic planes. Such a constructive interference can be obtained only for specific directions of the incident and diffracted beams (Bragg phase-matching condition). When the number of diffracting planes increases, the phase-matching condition becomes more and more stringent, and the angular dispersion of the diffracted beam goes down to the diffraction limit. The striking difference between Bragg diffraction in solid-state physics and in optical lattices, comes from the four orders of magnitude that separate the spatial periods. In solid-state physics, the diffracted beams are in the x-ray range, while in optical lattices visible or near-infrared light is used.

Bragg condition and optical lattices. In its general form, the Bragg condition stipulates that the change in wavevector of the light coincides with a vector of the reciprocal lattice [109]. In the optical lattices, a basis of the reciprocal lattice is given by the differences between the wavevectors of the trapping beams [55, 56]. For a given vector $\boldsymbol{K}_0$ of the reciprocal lattice, the wavevectors $\boldsymbol{k}_i$ and $\boldsymbol{k}_d$ of the incident and diffracted beams that satisfy the Bragg condition define a cone of axis $\boldsymbol{K}_0$ (figure 15). If the detection light has the same wavelength λ_b as the trapping light λ_L, the only vectors of the reciprocal lattice that may allow a Bragg diffraction are those with a length smaller than $2k_L$. In order to generate a Bragg diffracted beam, the propagation direction of the probe has to be on one of the allowed cones. One particular case is obtained for the cones defined by each pair of trapping beams; this result shows that a trapping beam can be diffracted in the direction of each of the other trapping beams [56, 110].

Four-wave mixing versus Bragg diffraction. As already mentioned, the Bragg condition and the phase-matching condition coincide in the case of optical lattices. At first glance, it seems that this fact forbids one to consider Bragg diffraction as a proof of the long-range order in optical lattices [56], because the four-wave mixing is present even in disordered samples. However, two different approaches can be used to overcome this ambiguity. One possibility is to turn off the trapping beams before detecting the Bragg diffraction signal [107]. The only observable that survives long enough is the atomic density and the probe beam tests the spatial order of the sample. Another possibility is to use a probe beam that is detuned with respect to the trapping beams [62, 108, 111]. In this case the resulting interference pattern moves quickly in the sample, and no polarization grating can build up. The four-wave mixing component is then much weaker than the Bragg diffraction signal arising from the static density grating.

Bragg diffraction as a diagnostic tool. Bragg-diffracted intensity is very sensitive to the details of the atomic density distribution in the optical lattice. For instance, an increase of the dispersion $\Delta\zeta^2$ of the atoms around their equilibrium positions will decrease the Bragg signal by the Debye–Waller factor $\exp(-K^2\Delta\zeta^2)$. This dependence allows the precise observation of the dynamics of the cooling and localization process either in 1D or 3D optical lattices by following the time evolution of the Bragg signal [112]. The same kind of measurements give information on the motion of the atomic wavepacket at the bottom of the potential wells when the potential is time modulated [113]. This modulation can be induced by an extra probe beam that excites the oscillation of the atoms at the bottom of the wells. The stimulated Raman transitions in this case put the atoms in higher vibrational levels, leading to a decrease in the Bragg-diffracted intensity [111]. Bragg diffraction is also sensitive to the change in refractive index due to the presence of the trapped atoms [107, 110, 111].

5.4. Velocimetry of the cold sample

Accurate momentum distribution characterization is probably the first and most important diagnostic tool introduced in laser-cooling experiments. In the case of optical lattices, knowledge of the optical potential features allows the linking of the momentum distribution to the position distribution. In this way, a velocimetry technique can give information about the spatial spread in the optical potential wells. The simplest method measures the 1D (vertical) temperature by a time-of-flight diagnostic. More elaborate imaging techniques allow the observation of anisotropic momentum distributions along two distinct directions. Finally, sophisticated velocity selection methods are capable of a very precise evaluation of the momentum distribution.

The time-of-flight technique. The time-of-flight diagnostic, developed for the optical molasses [27, 114], gives the vertical temperature of an atomic sample. Its principle is very simple: the trapping beams are turned off and the atoms fall down because of gravity. During the falling time, the width of the cloud increases because of the initial momentum distribution. At a given distance below the trap, the cloud crosses a resonant light sheet and the arrival time distribution can be recorded by a fluorescence or absorption measurement. Assuming a Gaussian distribution for the initial momentum and position spreads, the arrival time distribution is also Gaussian if the falling time is long enough. The initial temperature is obtained by a simple relation between the widths of the initial Gaussian distributions ($\sigma_{p_z}^2 = Mk_BT_z$ and σ_z), the falling time t_f, the width of the arrival time σ_t, and the width of the vertical profile of the light sheet σ_{sheet}:

$$T_z = \frac{M}{k_B}(g^2\sigma_t^2 - (\sigma_z^2 + \sigma_{sheet}^2)/t_f^2)$$

The main problem with this technique is that it requires precise knowledge of the initial size of the cloud, especially in the case of low initial temperatures. A way to circumvent this problem is to measure the time of flight with two spatially separated light sheets. In this case, a proper analysis of the measured temporal widths cancels the spatial spread of the initial cloud. The other critical point is the rate at which the trapping beams are turned off. If they are turned off slowly, the atoms adiabatically follow the change in intensity and the measured quantities are related to an intermediate situation when the adiabatic following breaks down.

Imaging techniques. The 1D time-of-flight technique can be generalized by imaging techniques [115] in order to obtain momentum distributions along several directions. The principle is the same: one records the increase of the cloud size after a given time of free expansion. Images of the sample are obtained by flashing the atomic cloud with a resonant beam pulse. It is then possible either to obtain a fluorescence image or to measure the spatial profile of the cloud absorption hollowed-out in the flash beam (shadow images). The comparison between the image obtained at the turning-off time and another obtained later allows the full reconstruction of a 2D momentum distribution. In a recent experiment [47, 51] this technique allowed the observation of the momentum distribution associated to different vibrational states in a 1D optical lattice.

These imaging techniques have been also used to directly observe the atomic localization in holographic optical lattices [64] and in Sisyphus optical super-lattices [61]. An improved version of the technique has been developed in order to observe the dynamics of Bose–Einstein condensated samples [116]: instead of using resonant flash beams it is possible to obtain a phase image of the sample with a non-resonant flash, introducing then a non-destructive diagnostic tool.

Other velocimetry techniques. The time-of-flight technique requires an expansion of the atomic cloud and the resolution limit increases with the free evolution time. In some experimental situations, a very fine resolution is required and/or there is not enough room for a big expansion. In such cases, there are two other velocimetry techniques that can be used.

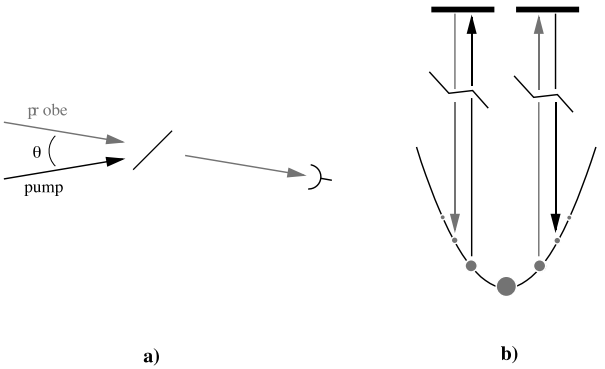

Figure 16. Recoil-induced resonance in a free-atom cloud. (*a*) Detection configuration: two beams define a small angle θ and the probe transmission is monitored. (*b*) Raman transitions between different momentum states. Population differences (populations are represented by the dimensions of the grey discs) induce a probe amplification for $\delta < 0$ and a probe absorption for $\delta > 0$.

The first technique is based on the recoil-induced resonance, a physical effect analogous to the gain mechanism in free-electron lasers [104]. In this case a pump and a probe nearly co-propagating interact with a cloud of free atoms (figure 16). Analysed in the momentum basis, the absorption of a pump photon followed by the stimulated emission of a probe photon can be viewed as a Raman transition between two states with different transverse momenta. In the limit of small angles θ between pump and probe directions, the momentum transfer is $\hbar k_L\theta$. Depending on the pump–probe detuning δ, energy and momentum conservation imply that only the atoms having a transverse momentum $p_{transv} = \frac{M\delta}{k_L\theta}$ are resonantly excited. As the Raman transition cross section is affected by the population difference between the initial and final states, the transmission spectrum of the probe (as a function of δ) is proportional to the derivative of the momentum distribution†. A direct comparison between this technique and the time-of-flight technique proved its validity [117].

The second technique is Raman velocimetry. Its basic principle is exactly the same as the Raman cooling process for free atoms: velocity-selective Raman transitions. If at the starting point all the atoms in the atomic sample are in the less energetic stable state, we can selectively transfer one velocity class to the upper one with a Raman pulse. The width of this velocity class is determined simply by the pulse duration and, for caesium atoms, can be as low as $v_{rec}/16$. A light flash can then excite these atoms from the upper stable state to the excited state where they can be detected by collecting the fluorescence. In order to obtain the entire velocity distribution, one has to repeat this measure for each velocity class; nevertheless, this method is the most powerful one. It allowed, for example, the measurement of Bloch oscillations in a periodic 1D optical lattice [9].

† This relationship is valid as long as the momentum distribution width is greater than the photon momentum $\hbar k_L$.

6. Conclusion

Fine control of the atomic external degrees of freedom allowed the development of a new field in atomic physics: the study of optical lattices. Such systems display very peculiar characteristics that make them similar to solid-state crystals, but with the flexibility of an intrinsically pure and defectless atomic sample. This analogy is very important, but it is also interesting to display the differences between these two classes of systems. First of all, dissipative processes in optical lattices kill the coherence of the atomic wavefunction. In a similar, but not identical, way the defects in solid-state samples also destroy the electronic wavefunction spatial coherence. The optical lattices can be made 'defectless' by reducing the spontaneous emission (far-detuned regime)†. The second difference is the electron–electron interaction which is a dominant relaxation mechanism in solids and which is usually absent in optical lattices. This absence has two reasons: the fact that atoms are neutral (the interaction range and strength are reduced) and the traditionally low densities obtained in optical lattices (one lattice site in 100 is effectively occupied in a standard 3D Sisyphus optical lattice). In a recent experiment [119] the second limitation was overcome, allowing the observation of strong atom–atom interactions in a single optical potential well. Finally, the phonon–electron interaction is virtually absent in optical lattices because the optical potential is imposed by the beam geometry and does not vibrate (however, some recent experiments [111] report on the back-action of the atoms on the trapping field). In any case, the precise control of the atomic positions (eventually associated to an internal-state control) allows, in principle, a fine study of collisional processes [120, 121] and, eventually, the *in situ* production of molecular lattices [122].

The demonstration of Bose–Einstein condensation [5] opened new perspectives to the study of optical lattices (as to the whole laser-cooling field). In particular, two strategies are now extensively explored: the use of a condensed cloud (obtained by 'standard' evaporative cooling) as a source for optical lattice experiments [11, 123–125] and the search for quantum degeneracy directly inside an optical lattice [54, 119]. As a future evolution of the first option one can cite, for instance, atomic lithography with a bright coherent atomic beam ('atomic laser') which will probably lead to a technological breakthrough. For the second option, Raman sideband cooling coupled to far-detuned lattices seems to be the most promising path for development.

In conclusion, the optical lattices of neutral atoms couple a strong fundamental interest (e.g. the study of the problem of quantum transport) to multiple practical perspectives (atomic lithography, quantum computing [126, 127], etc). This 'new state of matter' has far from opened all its secrets and potentialities; we hope that the next ten years will see another spectacular increase in the knowledge of this new exciting field.

† A study of the effect of decoherence has been performed taking advantage of this dependence [118].

Acknowledgments

This introductory tutorial derives in part from a PhD thesis [88] undertaken at the Laboratoire Kastler Brossel, 'unité de recherche de l'Ecole Normale Supérieure et de l'Université Pierre et Marie Curie, associée au CNRS'. The authors are indebted to many members of this institution for repeated and fruitful seminars and discussions. Among them, the authors want especially to thank C Cohen-Tannoudji, G Grynberg, J-Y Courtois, C Triché and K I Petsas. Special thanks also to E Arimondo for encouraging us to write this tutorial. The authors want finally to thank the anonymous referee for his remarks and suggestions that contributed to the improvement of the manuscript. LG gratefully acknowledges the financial support from the European Community (Contract No ERBCHBI-CT-94-1690) and from the Collège de France.

The Laboratoire de Physique des Lasers, Atomes et Molécules is 'Unité de Recherche de l'Université de Lille 1 et du CNRS (UMR8523)'. The Centre d'Etudes et de Recherches Lasers et Applications (CERLA) is supported by the Ministère chargé de la Recherche, the Région Nord-Pas de Calais and the Fonds Européen de Développement Economique des Régions.

References

[1] Cagnac B, Plimmer M D, Julien L and Biraben F 1994 The hydrogen atom, a tool for metrology *Rep. Prog. Phys.* **57** 853
[2] Chu S 1998 The manipulation of neutral particles *Rev. Mod. Phys.* **70** 685
[3] Cohen-Tannoudji C 1998 Manipulating atoms with photons *Phys. Scr.* T **76** 33
[4] Phillips W D 1998 Laser cooling and trapping of neutral atoms *Rev. Mod. Phys.* **70** 721
[5] Anderson M H, Ensher J H, Mathews M R, Wieman C E and Cornell E A 1995 Observation of Bose–Einstein condensation in a dilute atomic vapor *Science* **269** 198
[6] Meacher D R 1998 Optical lattices—crystalline structures bound by light *Contemp. Phys.* **39** 329
[7] Jessen P S and Deutsch I H 1996 *Adv. At. Mol. Opt. Phys.* **37** 95
[8] Grynberg G and Triché C 1996 Atoms in optical lattices *Coherent and Collective Interactions of Particles and Radiation Beams: Proc. Int. School of Physics Enrico Fermi, Course CXXXI (Varenna, 1995)* ed A Aspect, W Barletta and R Bonifacio (Amsterdam: North-Holland) pp 243
[9] BenDahan M, Peik E, Reichel J, Castin Y and Salomon C 1996 Bloch oscillations of atoms in an optical potential *Phys. Rev. Lett.* **76** 4508
[10] Wilkinson S, Barucha C, Madison K, Niu Q and Raizen M 1996 Observation of atomic Wannier–Stark ladders in an accelerating optical potential *Phys. Rev. Lett.* **76** 4512
[11] Anderson B P and Kasevich M A 1998 Macroscopic quantum interference from atomic tunnel arrays *Science* **282** 1686
[12] Madison K W, Fischer M C, Diener R B, Niu Q and Raizen M G 1998 Dynamical bloch band suppression in an optical lattice *Phys. Rev. Lett.* **81** 5093
[13] Raizen M, Salomon C and Niu Q 1997 New light on quantum transport *Phys. Today* **50** (7) 30
[14] Behringer R H, Natarajan V and Timp G 1995 Laser focused atomic deposition: a new lithography tool *Appl. Phys. Lett.* **68** 1034

[15] Brezger B, Schulze T, Drodofsky U, Stuhler J, Nowak S, Pfau T and Mlynek J 1997 Nanolithography with neutral chromium and helium atoms *J. Vac. Sci. Technol.* B **15** 2905

[16] Frisch O R 1933 Experimenteller nachweis des einsteinischen strahlungsrückstosses *Z. Phys.* **86** 42

[17] Hänsch T W and Schawlow A L 1975 Cooling of gases by laser radiation *Opt. Commun.* **13** 68

[18] Wineland D and Dehmelt H 1975 Proposed $10^{14}\Delta\nu < \nu$ laser fluorescence spectroscopy on Tl^+ mono-ion oscillator III *Bull. Am. Phys. Soc.* **20** 637

[19] Stenholm S 1986 The semiclasical theory of laser cooling *Rev. Mod. Phys.* **58** 699

[20] Chu S, Hollberg L, Bjorkholm J E, Cable A and Ashkin A 1985 Three-dimensional viscous confinement and cooling of atoms by resonance radiation pressure *Phys. Rev. Lett.* **55** 48

[21] Minogin V G and Javanainen J 1982 A tetraedral light pressure trap for atoms *Opt. Commun.* **43** 119

[22] Ashkin A and Gordon J P 1983 Stability of radiation-pressure particle traps: an optical Earnshaw theorem *Opt. Lett.* **8** 511

[23] Cohen-Tannoudji C 1962 Théorie quantique du cycle de pompage optique *Ann. Phys., Paris* **7** 423

[24] Pritchard D E, Raab E L, Bagnato V, Wieman C E and Watts R N 1986 Light traps using spontaneous forces *Phys. Rev. Lett.* **57** 310

[25] Raab E L, Prentiss M, Cable A, Chu S and Pritchard D E 1987 Trapping of neutral sodium atoms with radiation pressure *Phys. Rev. Lett.* **59** 2631

[26] Monroe C, Swann W, Robinson H and Wieman C 1990 Very cold trapped atoms in a vapor cell *Phys. Rev. Lett.* **65** 1571

[27] Lett P D, Watts R N, Westbrook C I, Phillips W D, Gould P L and Metcalf H J 1988 Observation of atoms laser cooled below the Doppler limit *Phys. Rev. Lett.* **61** 169

[28] Dalibard J and Cohen-Tannoudji C 1989 Laser cooling below the Doppler limit by polarization gradients: simple theoretical models *J. Opt. Soc. Am.* B **6** 2023

[29] Ungar P J, Weiss D S, Riis E and Chu S 1989 Optical molasses and multilevel atoms: theory *J. Opt. Soc. Am.* B **6** 2058

[30] Castin Y and Dalibard J 1991 Quantization of atomic motion in optical molasses *Europhys. Lett.* **14** 761

[31] Marte P, Dum R, Taïeb R, Zoller P, Shahriar M S and Prentiss M 1994 Polarization-gradient-assisted subrecoil cooling: quantum calculations in one dimension *Phys. Rev.* A **49** 4826

[32] Weidemüller M, Esslinger T, Ol'shanii M A, Hemmerich A and Hänsch T W 1994 A novel scheme for efficient cooling below the photon recoil limit *Europhys. Lett.* **27** 109

[33] Grynberg G and Courtois J-Y 1994 Proposal for a magneto-optical lattice for trapping atoms in nearly-dark states *Europhys. Lett.* **27** 41

[34] Aspect A, Arimondo E, Kaiser R, Vansteenkiste N and Cohen-Tannoudji C 1988 Laser cooling below the one-photon recoil energy by velocity-selective coherent population trapping *Phys. Rev. Lett.* **61** 826

[35] Lawall J, Kulin S, Saubamea B, Bigelow N, Leduc M and Cohen-Tannoudji C 1995 Three-dimensional laser cooling of helium beyond the single-photon recoil limit *Phys. Rev. Lett.* **75** 4195

[36] Kasevich M and Chu S 1992 Laser cooling below a photon recoil with three level atoms *Phys. Rev. Lett.* **69** 1741

[37] Reichel J, Bardou F, BenDahan M, Peik E, Rand S, Salomon C and Cohen-Tannoudji C 1995 Raman cooling below 3 nK: new approach inspired by Levy flights statistics *Phys. Rev. Lett.* **75** 4575

[38] Saubamea B, Hijmans T W, Kulin S, Rasel E, Peik E, Leduc M and Cohen-Tannoudji C 1997 Direct measurement of the spatial correlation function of ultracold atoms *Phys. Rev. Lett.* **79** 3146

[39] Cohen-Tannoudji C 1992 Atomic motion in laser light *Fundamental Systems in Quantum Optics (Les Houches 1990, Session LIII)* ed J Dalibard, J-M Raimond, and J Zinn-Justin (Amsterdam: Elsevier) p 1

[40] Verkerk P, Lounis B, Salomon C, Cohen-Tannoudji C, Courtois J-Y and Grynberg G 1992 Dynamics and spatial order of cold caesium atoms in a periodic optical potential *Phys. Rev. Lett.* **68** 3861

[41] Jessen P S, Gerz C, Lett P D, Phillips W D, Rolston S L, Spreeuw R J C and Westbrook C I 1992 Observation of quantized motion of Rb atoms in an optical field *Phys. Rev. Lett.* **69** 49

[42] Triché C 1997 *PhD Thesis* École Polytechnique, Palaiseau

[43] Müller-Seydlitz T, Hartl M, Brezger B, Hänsel H, Keller C, Schnetz A, Spreeuw R J C, Pfau T and Mlynek J 1997 Atoms in the lowest motional band of a three-dimensional optical lattice *Phys. Rev. Lett.* **78** 1038

[44] Hemmerich A, Weidemüller M, Esslinger T, Zimmermann C and Hänsch T W 1995 Trapping atoms in a dark optical lattice *Phys. Rev. Lett.* **75** 37

[45] Mennerat-Robilliard C, Lucas D, Guibal S, Tabosa J, Jurczak C, Courtois J-Y and Grynberg G 1999 Ratchet for cold rubidium atoms: the asymmetric optical lattice *Phys. Rev. Lett.* **82** 851

[46] Sheehy B, Shang S Q, Straten P V D, Hatamian S and Metcalf H 1990 Magnetic-field-induced laser cooling below the Doppler limit *Phys. Rev. Lett.* **64** 858

[47] Perrin H, Kuhn A, Bouchoule I and Salomon C 1998 Sideband cooling of neutral atoms in a far-detuned optical lattice *Europhys. Lett.* **42** 395

[48] Winoto S L, DePue M T, Bramall N E and Weiss D S 1999 Laser cooling at high density in deep far-detuned optical lattices *Phys. Rev.* A **59** R19

[49] Hamann S E, Haycock D L, Klose G, Pax P H, Deutsch I H and Jessen P S 1998 Resolved-sideband raman cooling to the ground state of an optical lattice *Phys. Rev. Lett.* **80** 4149

[50] Vuletic V, Chin C, Kerman A J and Chu S 1998 Degenerate sideband cooling of trapped cesium atoms at very high atomic densities *Phys. Rev. Lett.* **81** 5768

[51] Bouchoule I, Perrin H, Kuhn A, Morinaga M and Salomon C 1999 Neutral atoms prepared in Fock states of a one-dimensional harmonic potential *Phys. Rev.* A **59** R8

[52] Courtois J-Y and Grynberg G 1992 Probe transmission in one-dimensional optical molasses: theory for linearly cross-polarized cooling beams *Phys. Rev.* A **46** 7060

[53] Marte P, Dum R, Taïeb R, Lett P D and Zoller P 1993 Quantum wave function simulation of the resonance fluorescence spectrum from one-dimensional optical molasses *Phys. Rev. Lett.* **71** 1335

[54] Vuletic V, Kerman A J, Chin C and Chu S 1999 Observation of low-field feshbach resonances in collisions of cesium atoms *Phys. Rev. Lett.* **82** 1406

[55] Petsas K I, Coates A B and Grynberg G 1994 Crystallography of optical lattices *Phys. Rev.* A **50** 5173

[56] Grynberg G, Lounis B, Verkerk P, Courtois J-Y and Salomon C 1993 Quantized motion of cold caesium atoms in two- and three-dimensional optical potentials *Phys. Rev. Lett.* **70** 2249

[57] Hemmerich A and Hänsch T W 1993 Two-dimensional atomic crystal bound by light *Phys. Rev. Lett.* **70** 410

[58] Castin Y, Berg-Sørensen K, Dalibard J and Mølmer K 1994 Two-dimensional Sisyphus cooling *Phys. Rev.* A **50** 5092

[59] Guidoni L, Triché C, Verkerk P and Grynberg G 1997 Trapping and cooling caesium atoms in a quasi-periodic optical lattice *Trends in Optics and Photonics : Ultracold Atoms and Bose–Einstein-Condensation* ed K Burnett (Washington, DC: Optical Society of America) p 77

[60] Hippert F and Gratias D (ed) 1994 *Lectures on Quasicrystals* (Paris: Les Editions de Physique)

[61] Guidoni L and Verkerk P 1998 Direct observation of atomic

localization in optical superlattices *Phys. Rev.* A **57** R1501
[62] Guidoni L, Triché C, Verkerk P and Grynberg G 1997 Quasiperiodic optical lattices *Phys. Rev. Lett.* **79** 3363
[63] Guidoni L, Dépret B, di Stefano A and Verkerk P 1999 Atomic diffusion in an optical quasicrystal with fivefold symmetry *Phys. Rev.* A **50** in press
[64] Boiron D, Michaud A, Fournier J-M, Simard L, Sprenger M, Grynberg G and Salomon C 19998 Cold and dense caesium clouds in far-detuned dipole traps *Phys. Rev.* A **57** R4106
[65] Mennerat-Robilliard C, Boiron D, Fournier J M, Aradian A, Horak P and Grynberg G 1998 Cooling caesium atoms in a Talbot lattice *Europhys. Lett.* **44** 442
[66] Horak P, Courtois J-Y and Grynberg G 1998 Atom cooling and trapping by disorder *Phys. Rev.* A **58** 3953
[67] Boiron D, Mennerat-Robilliard C, Fournier J-M, Guidoni L, Salomon C and Grynberg G 1999 Trapping and cooling cesium atoms in a speckle field *Europhys. J.* D in press
[68] Barrat J-P and Cohen-Tannoudji C 1961 Etude du pompage optique dans le formalisme de la matrice densité *J. Phys.* (Paris) **22** 329
[69] Mølmer K 1991 Friction and diffusion coefficients for cooling of atoms in laser fields with multidimensional periodicity *Phys. Rev.* A **44** 5820
[70] Javanainen J 1994 Polarization gradient cooling in three dimensions: comparison of theory and experiment *J. Phys. B: At. Mol. Opt. Phys.* **27** L47
[71] Hodapp T W, Gerz C, Furthlehner C, Westbrook C I, Phillips W D and Dalibard J 1995 Spatial diffusion in 3D optical molasses *Appl. Phys.* B **60** 135
[72] Marksteiner S, Ellinger K and Zoller P 1996 Anomalous diffusion and Lévy walks in optical lattices *Phys. Rev.* A **53** 3409
[73] Castin Y 1992 *PhD Thesis* Université Pierre et Marie Curie, Paris
[74] Petsas K I, Courtois J-Y and Grynberg G 1996 Temperature and magnetism of gray optical lattices *Phys. Rev.* A **53** 2533
[75] Deutsch I H, Grondalski J and Alsing P M 1997 Local dynamics of laser cooling in an optical lattice *Phys. Rev.* A **56** R1705
[76] Deutsch I H and Jessen P S 1998 Quantum-state control in optical lattices *Phys. Rev.* A **57** 1972
[77] Berg-Sørensen K 1994 Two-dimensional Sisyphus cooling in a three-beam laser configuration *Phys. Rev.* A **49** R4297
[78] Dalibard J, Castin Y and Mølmer K 1992 Wave-function approach to dissipative processes in quantum optics *Phys. Rev. Lett.* **68** 580
[79] Dum R, Zoller P and Ritsch H 1992 Monte Carlo simulation of the atomic master equation for spontaneous emission *Phys. Rev.* A **45** 4879
[80] Marte P, Dum R, Taïeb R and Zoller P 1993 Resonance fluorescence from quantized one-dimensional molasses *Phys. Rev.* A **47** 1378
[81] Taïeb R, Marte P, Dum R, and Zoller P 1993 Spectrum of resonance fluorescence and cooling dynamics in quantized one dimensional molasses: effects of laser configuration *Phys. Rev.* A **47** 4986
[82] Castin Y and Mølmer K 1995 Monte Carlo wavefunction analysis of 3D optical molasses *Phys. Rev. Lett.* **74** 3772
[83] Raithel G, Phillips W D and Rolston S L 1998 Magnetization and spin-flip dynamics of atoms in optical lattices *Phys. Rev.* A **58** R2660
[84] Raithel G, Phillips W D and Rolston S L 1998 Collapse and revivals of wave packets in optical lattices *Phys. Rev. Lett.* **81** 3615
[85] Horak P and Ritsch H 1997 Self-induced Bragg-type scattering in dark optical superlattices *Phys. Rev.* A **55** 2176
[86] Courtois J-Y, Guibal S, Meacher D R, Verkerk P and Grynberg G 1996 Propagating elementary excitation in a dilute optical lattice *Phys. Rev. Lett.* **77** 40
[87] Guibal S, Mennerat-Robilliard C, Larousserie D, Triché C, Courtois J-Y and Grynberg G 1997 Radiation pressure in a rubidium optical lattice: an atomic analog to the photorefractive effect *Phys. Rev. Lett.* **78** 4709
[88] Guidoni L 1998 *PhD Thesis* Université Pierre et Marie Curie, Paris
[89] Petsas K I, Grynberg G and Courtois J-Y 1999 Semiclassical Monte Carlo approaches for realistic atoms in optical lattices *Eur. Phys. J.* D **6** 29
[90] Jurczak C, Desruelle B, Sengstock K, Courtois J-Y, Westbrook C I and Aspect A 1996 Atomic transport in an optical lattice: an investigation through polarization-selective intensity correlations *Phys. Rev. Lett.* **77** 1727
[91] Rudy P, Ejnisman E and Bigelow N P 1998 Fluorescence Investigation of parametrically excited motional wave packets in optical lattices *Phys. Rev. Lett.* **78** 4906
[92] Grison D, Lounis B, Salomon C, Courtois J-Y and Grynberg G 1991 Raman spectroscopy of caesium atoms in a laser trap *Europhys. Lett.* **15** 149
[93] Boyd R W 1992 *Nonlinear Optics* (Boston, MA: Academic)
[94] Lounis B, Verkerk P, Courtois J-Y, Salomon C and Grynberg G 1993 Quantized atomic motion in 1D caesium molasses with magnetic field *Europhys. Lett.* **21** 13
[95] Hemmerich A, Zimmermann C and Hänsch T W 1993 Sub-kHz Rayleigh resonance in a cubic atomic crystal *Europhys. Lett.* **22** 89
[96] Verkerk P, Meacher D R, Coates A B, Courtois J-Y, Guibal S, Lounis B, Salomon C and Grynberg G 1994 Designing 3D optical lattices—an investigation with caesium atoms *Europhys. Lett.* **26** 171
[97] Courtois J-Y 1996 Novel stimulated scattering process in optical lattices *Coherent and Collective Interactions of Particles and Radiation Beams: Proc. Int. School of Physics Enrico Fermi, Course CXXXI (Varenna, 1995)* ed A Aspect, W Barletta and R Bonifacio (Amsterdam: North-Holland) p 341
[98] Grynberg G, Vallet M and Pinard M 1990 Redistribution of photons and frequency mixing with cross-polarized beams in sodium *Phys. Rev. Lett.* **65** 701
[99] Jurczak C, Courtois J-Y, Desruelle B, Westbrook C I and Aspect A 1998 Spontaneous light scattering from propagating density fluctuations in an optical lattice *Eur. Phys. J.* D **1** 53
[100] Triché C, Guidoni L, Verkerk P and Grynberg G 1997 Coherent transients in optical lattices *Trends in Optics and Photonics: Ultracold Atoms and Bose–Einstein-Condensation* ed K Burnett (Washington, DC: Optical Society of America) p 82
[101] Kozuma M, Nakagawa K, Jhe W and Ohtsu M 1996 Observation of temporal behaviour of an atomic wave packet localized in an optical potential *Phys. Rev. Lett.* **76** 2428
[102] Phillips W D and Westbrook C I 1997 Comment on observation of temporal behaviour of an atomic wave packet localized in an optical potential *Phys. Rev. Lett.* **78** 2676
[103] Kozuma M, Nakagawa K, Jhe W and Ohtsu M 1997 Reply to the comment in *Phys. Rev. Lett.* **78** 2676 *Phys. Rev. Lett.* **78** 2677
[104] Courtois J-Y, Grynberg G, Lounis B and Verkerk P 1996 Recoil-induced resonances in caesium: an atomic analog to the free-electron laser *Phys. Rev. Lett.* **72** 3017
[105] Westbrook C I, Watts R N, Tanner C E, Rolston S L, Phillips W D, Lett P D and Gould P L 1990 Localization of atoms in a three-dimensional standing wave *Phys. Rev. Lett.* **65** 33
[106] Gatzke M, Birkl G, Jessen P S, Katsberg A, Rolston S L and Phillips W D 1997 Temperature and localization of atoms in three-dimensional optical lattices *Phys. Rev.* A

55 R3987
[107] Birkl G, Gatzke M, Deutsch I H, Rolston S L and Phillips W D 1995 Bragg scattering from atoms in optical lattices *Phys. Rev. Lett.* **75** 2823
[108] Weidemüller M, Hemmerich A, Görlitz A, Esslinger T and Hänsch T W 1995 Bragg diffraction in an atomic lattice bound by light *Phys. Rev. Lett.* **75** 4583
[109] Ashcroft N W and Mermin N D 1976 *Solid State Physics* (New York: Holt, Rinehart and Winston)
[110] Deutsch I H, Spreeuw R J C, Rolston S L and Phillips W D 1995 Photonic band gaps in optical lattices *Phys. Rev.* A **52** 1394
[111] Weidemüller M, Görlitz A, Hänsch T W and Hemmerich A 1998 Local and global properties of light-bound atomic lattices investigated by Bragg diffraction *Phys. Rev.* A **58** 4647
[112] Raithel G, Birkl G, Katsberg A, Phillips W D and Rolston S L 1997 Cooling and localization dynamics in optical lattices *Phys. Rev. Lett.* **78** 630
[113] Raithel G, Birkl G, Phillips W D and Rolston S L 1997 Compression and parametric driving of atoms in optical lattices *Phys. Rev. Lett.* **78** 2928
[114] Salomon C, Dalibard J, Phillips W D, Clairon A and Guellati S 1990 Laser cooling of caesium atoms below 3 μK *Europhys. Lett.* **12** 683
[115] Walhout M, Sterr U, Orzel C, Hoogerland M and Rolston S L 1995 Optical control of ultracold collisions in metastable xenon *Phys. Rev. Lett.* **74** 506
[116] Andrews M R, Mewes M O, van Druten N J, Durfee D S, Kurn D M and Ketterle W 1996 Direct, nondestructive observation of a bose condensate *Science* **273** 84
[117] Meacher D R, Boiron D, Metcalf H, Salomon C and Grynberg G 1994 Method for velocimetry of cold atoms *Phys. Rev.* A **50** R1992
[118] Klappauf B G, Oskay W H, Steck D A and Raizen M G 1998 Observation of noise and dissipation effects on dynamical localization *Phys. Rev. Lett.* **81** 1203
[119] DePue M T, McKormick C, Winoto S L, Oliver S and Weiss D S 1999 Unity occupation of sites in a 3D optical lattice *Phys. Rev. Lett.* **82** 2262
[120] Kunugita H, Ido T and Shimizu F 1997 Ionizing collisional rate of metastable rare-gas atoms in an optical lattice *Phys. Rev. Lett.* **79** 621
[121] Lawall J, Orzel C and Rolston S L 1998 Suppression and enhancement of collisions in optical lattices *Phys. Rev. Lett.* **80** 480
[122] Fioretti A, Comparat D, Crubellier A, Dulieu O, Masnou-Seeuws F and Pillet P 1998 formation of cold Cs_2 molecules through photoassociation *Phys. Rev. Lett.* **80** 4402
[123] Jaksch D, Bruder C, Cirac J I, Gardiner C W and Zoller P 1998 Cold bosonic atoms in optical lattices *Phys. Rev. Lett.* **81** 3108
[124] Berg-Sørensen K and Mølmer K 1998 Bose–Einstein condensates in spatially periodic potentials *Phys. Rev.* A **58** 1480
[125] Choi D I and Niu Q 1999 Bose–Einstein condensates in an optical lattice 1999 *Phys. Rev. Lett.* **82** 2022
[126] Brennen G B, Caves C M, Jessen P S and Deutsch I H 1999 Quantum logic gates in optical lattices *Phys. Rev. Lett.* **82** 1060
[127] Jaksch D, Briegel H-J, Cirac J I, Gardiner C W and Zoller P 1999 Entanglement of atoms via cold controlled collisions *Phys. Rev. Lett.* **82** 1975